

## Review of Candidate Techniques for Material Accountancy Measurements in Electrochemical Separations Facilities

Jamie B. Coble, Steven E. Skutnik, S. Nathan Gilliam & Michael P. Cooper

To cite this article: Jamie B. Coble, Steven E. Skutnik, S. Nathan Gilliam & Michael P. Cooper (2020): Review of Candidate Techniques for Material Accountancy Measurements in Electrochemical Separations Facilities, Nuclear Technology, DOI: [10.1080/00295450.2020.1724728](https://doi.org/10.1080/00295450.2020.1724728)

To link to this article: <https://doi.org/10.1080/00295450.2020.1724728>



© 2020 The Author(s). Published with license by Taylor & Francis Group, LLC.



Published online: 10 Apr 2020.



Submit your article to this journal [↗](#)



Article views: 348




View related articles [↗](#)



View Crossmark data [↗](#)



# Review of Candidate Techniques for Material Accountancy Measurements in Electrochemical Separations Facilities

Jamie B. Coble,\* Steven E. Skutnik, S. Nathan Gilliam, and Michael P. Cooper

*University of Tennessee–Knoxville, Nuclear Engineering Department, Nuclear Engineering Building, Knoxville, Tennessee 37996*

Received September 19, 2019

Accepted for Publication January 29, 2020

**Abstract** — *Electrochemical reprocessing (also commonly known as pyroprocessing) of used nuclear fuel is an alternative to aqueous reprocessing that confers a number of advantages, including the ability to process more recently discharged fuel, smaller resultant waste volumes, and the lack of isolation of plutonium in the product stream. While electrochemical reprocessing systems have seen a significant research and development effort, nuclear safeguards and the security of these systems remain underdeveloped, particularly given the significant differences in operating environment and process flow sheet compared with established aqueous methods. In this paper we present an overview of the current state of the art for several of the most promising candidate techniques for material accountancy and process monitoring measurements for electrochemical separations facilities for used nuclear fuel, specifically passive radiation signatures (gamma spectroscopy, neutron spectroscopy, alpha spectrometry, calorimetry, and microcalorimetry), active radiation signatures (X-ray interrogation and its derivatives, high-resolution X-ray, k-edge densitometry, and hybrid k-edge densitometry; laser-induced breakdown spectroscopy; active neutron interrogation and neutron coincidence counting; inductively coupled plasma mass spectrometry; and optical measurements such as ultraviolet visible spectroscopy, near-infrared spectroscopy, and Raman spectroscopy), and control and process state variable monitoring (cyclic voltammetry and bulk measurements such as level and density, load cell forces, and off-gas monitors). This assessment includes an evaluation of each measurement's respective modality (i.e., whether the measurement relates to elemental, isotopic, or other properties), published best estimates of measurement precision, measurement latency, and an overall evaluation of each technique's level of technical maturity. Additionally, this study assesses the most likely locations within the pyroprocessing flow sheet where measurements may be deployed, the physical information required to properly capture the behavior of such measurements, and potential modeling strategies for such measurements. This latter component thus serves to inform future development of process monitoring models in existing and proposed electrochemical separations simulation models.*

**Keywords** — *Pyroprocessing, electrochemical separations, material accountancy.*

**Note** — *Some figures may be in color only in the electronic version.*

---

\*E-mail: [jamie@utk.edu](mailto:jamie@utk.edu)

This is an Open Access article distributed under the terms of the Creative Commons Attribution-NonCommercial-NoDerivatives License (<http://creativecommons.org/licenses/by-nc-nd/4.0/>), which permits non-commercial re-use, distribution, and reproduction in any medium, provided the original work is properly cited, and is not altered, transformed, or built upon in any way.

## I. INTRODUCTION

Material control and accountancy (MC&A) programs at bulk handling facilities for special nuclear fuel (such as used fuel reprocessing facilities) are designed to detect and deter theft and illicit diversion of nuclear material. Current destructive assay approaches to MC&A are labor intensive and time consuming, often requiring samples be processed in a lab off site, resulting in sometimes significant delays between

sampling and results reporting. These traditional MC&A programs can be augmented with nondestructive assay (NDA) and online process monitoring to reduce resource requirements and improve the timeliness of MC&A and safeguards decisions at reprocessing facilities. Recent work by Garcia et al.<sup>1</sup> investigated the use of online process monitoring to detect protracted diversion scenarios using a variety of sensors, including salt density, off-gas flow, electric charge, solid metal density, passive radiation signatures, and product mass. This study showed the potential benefits of incorporating time and spatial indicators of system operation under a variety of monitoring deployment scenarios; results indicate that including high-reliability sensors that measure disparate indicators improves the overall performance of process monitoring systems for detecting facility misuse.<sup>1</sup>

At present, all commercial-scale facilities for used nuclear fuel (UNF) separations employ an aqueous reprocessing method, such as Plutonium URanium EXtraction (PUREX) or its derivatives.<sup>2</sup> Electrochemical reprocessing (also known as pyroprocessing) is an alternative method of nuclear fuel reprocessing that capitalizes on differences in Gibbs free energy to separate desired constituents of UNF for reuse, such as uranium, plutonium, americium, and curium. Using a eutectic salt mixture as a transfer medium, the desired products are electroplated as metallic dendrites on a solid cathode (uranium) or as intermetallic species onto a liquid metal cathode (uranium and transuranic species).<sup>3</sup> Because it does not generate a pure plutonium product (rather, plutonium is co-extracted with uranium and minor actinides), the resultant product streams may be less attractive for direct diversion for illicit proliferation purposes.

Several fundamental differences between the nature of aqueous reprocessing flow sheets and those proposed in pyroprocessing present substantial challenges to deploying current techniques developed for aqueous flow sheets directly to pyroprocessing systems. Briefly, pyroprocessing is a batch process, while PUREX is a continuous process. The hot-cell environments characteristic of pyroprocessing are likewise much harsher and more challenging for many in situ measurements. More important is the nature of material flows within the electrorefiner as compared to aqueous solvent extraction processes; unlike in the latter case, actinides that are not extracted during electrorefining remain in residence within the salt, resulting in a nonconstant residual inventory that can confound traditional material balance approaches.

Due to these and other differences between the two reprocessing methods, fundamentally different candidate online process monitoring and safeguards techniques are being developed for pyroprocessing, and existing approaches are being reevaluated with respect to their feasibility and applicability in a pyroprocessing setting.

This paper surveys existing and proposed measurement techniques for MC&A and process monitoring of pyroprocessing facilities, highlighting the relative maturity and technical feasibility of monitoring measurements. Rather than present an exhaustive review of each monitoring technology, we provide those details meant to guide researchers in selecting appropriate process monitoring and safeguards measurements to meet their own technical requirements. Fundamental and application-based references are given for each measurement method for the interested reader. [Section II](#) gives a brief overview of electrochemical reprocessing technology. Candidate in situ measurement modalities are summarized in [Sec. III](#). Because there is not a commercial-scale pyroprocessing facility available for safeguards and monitoring system development, near-term development of monitoring approaches will necessarily rely on modeling and simulation results. Potential simulation approaches for safeguards and process monitoring measurements in electrochemical simulation models are also discussed. The results of this landscape survey are summarized in [Sec. IV](#) along with some proposed areas of further research and development.

## II. ELECTROCHEMICAL REPROCESSING

Electrochemical reprocessing is a proposed alternative to the aqueous-based UNF separations processes deployed internationally. Unlike aqueous-based solvent extraction techniques (like PUREX), electrochemical separations rely on the differences in Gibbs free energy of chloride formation for metallic fuel and fission products to separate the UNF into reusable products. [Figure 1](#) summarizes the major stages of the pyroprocessing process.<sup>2</sup> At the head end of the process for oxide-based fuels, fuel assemblies are chopped and the cladding is removed. Uranium oxide (UO<sub>2</sub>) fuel pellets are then collected from the cladding and may be optionally processed in a voloxidation (volumetric oxidation) stage wherein the fuel is oxidized to form a U<sub>3</sub>O<sub>8</sub> powder,<sup>3,5</sup> with the net effect of both driving off certain volatile fission product species (e.g., noble gases and various fission products such as cesium, molybdenum, rhodium, ruthenium, tellurium, and technetium) as well as increasing the reaction surface area for the electroreduction stage.<sup>3</sup> The gaseous fission products are subsequently captured in the off-gas system and can be treated for inclusion in a consolidated ceramic waste form.

This U<sub>3</sub>O<sub>8</sub> powder is then lowered into an electro-reducer containing Li<sub>2</sub>O, whereupon the fuel is reduced to a metallic form by means of a cathodic reaction between the fuel-bearing basket and a platinum anode.

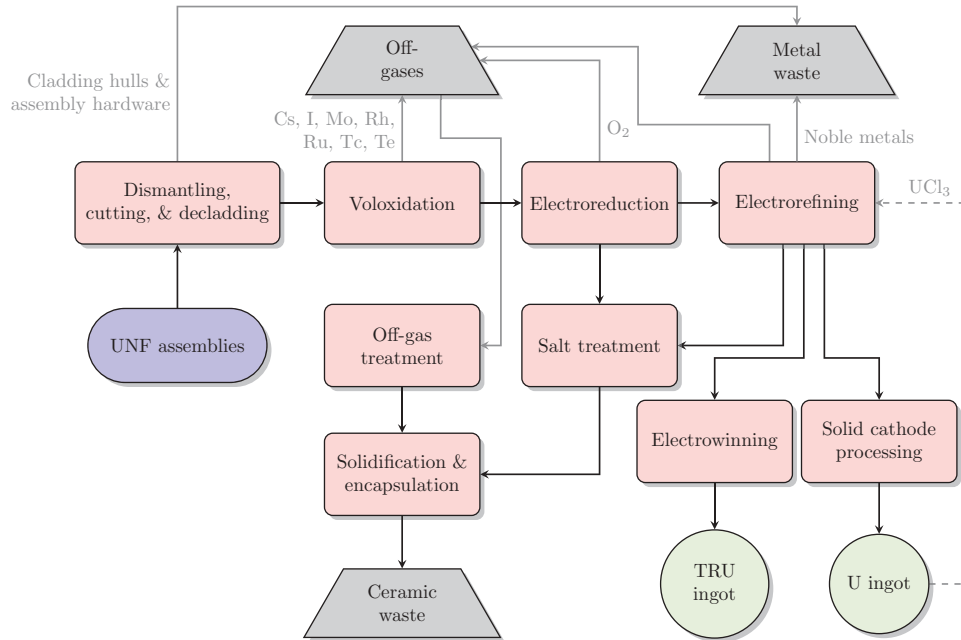


Fig. 1. Schematic of the electrochemical reprocessing flow sheet for UNF (adapted from Ref. 4). Primary material flows are indicated as solid lines; secondary flows are indicated by dashed lines (including recycling of uranium as  $UCl_3$  into the electrolyte salt). Following the electrorefiner process (which extracts uranium metal and optionally a U/TRU intermetallic), active metal species (i.e., lanthanides and alkali metals) are generally retained in the salt where they are processed into a ceramic waste form following salt treatment.<sup>3</sup> Conversely, noble metals (those that do not readily form chloride species) not collected with cladding hulls and assembly hardware remain in the anode basket and are recovered for casting as metal waste.<sup>3</sup>

As an electric potential is applied to the electrolytic cell in the electroreducer, lithium acts as a reducing agent, accumulating at the cathode and reducing the fuel to a metallic form.<sup>3,5</sup>

The newly formed metal chlorides are used as feed into the electrorefiner where recovery of uranium and transuranic radionuclides (TRUs) occurs. The fuel basket acts as an anode, where uranium and minor actinides form stable metallic chloride species based on their respective reduction potential and gradually diffuse into the salt.<sup>6</sup> From there, the deposition of uranium onto a solid cathode is controlled by adjusting the applied potential across the electrolytic cell in the electrorefiner. The alkaline and alkaline earth constituents form stable chlorides and thus stay within the salt throughout the refining process. The noble metals tend to stay in metallic form and remain in the anode basket due to having a lower Gibbs free energy for chloride formation.<sup>3,5</sup>

In certain pyroprocessing variants, a separate liquid cadmium cathode collects TRU elements along with remaining traces of uranium by adjusting the electrolytic cell voltage after the uranium dendrites are recovered. This is done to preserve the uranium content on the solid cathode and prevent contamination from TRUs. The molten salt that accompanies the uranium and TRU

products on their respective cathodes is then removed by vacuum distillation and undergoes a salt purification cycle. The uranium and TRUs are cast into metallic ingots in the cathode processor. This process also takes the remaining materials from the anode basket, such as undissolved actinides, salt, and noble metals, and loads them into a heated vacuum distillation furnace that is used to consolidate the metals into a metallic ingot waste form.

The electrochemical separations process greatly differs from that of aqueous methods, which introduces new challenges to online monitoring and safeguards. Aqueous reprocessing flow sheets consist of continuous, counter-current solvent extraction processes wherein material enters in one side and passes completely out the other end (either via the extracted product or as residual material left in the raffinate stream). In contrast, pyroprocessing is presently proposed as a batch process wherein the fuel enters the electrorefiner in a processing basket, the contents of which are then dissolved into the recirculated molten salt. Moreover, as the extraction rates of each elemental constituent are a direct function of their concentration within the salt, the residual inventories are not constant in time, introducing different system dynamics and time delays into the facility that must be accounted

for in an online monitoring and safeguards framework. As a result, traditional “mass balance” approaches (comparing measured inventories at the inlet and outlet streams) are difficult to implement without detailed knowledge of the content of the residual material left in the salt.

The issue of sampling and measurement further complicates accountancy measurements for electrochemical reprocessing systems. Unlike aqueous methods, pyroprocessing does not rely on chemical ligands (such as tri-*n*-butyl-phosphate) that are susceptible to degradation via radiolysis in high-radiation fields. Because of this, pyroprocessing allows for more recently discharged fuel to be processed. While advantageous from an operational standpoint (the same fuel would be substantially more difficult to process in an aqueous-based system and would likely be allowed longer cooling times before reprocessing), it introduces an additional challenge in terms of the intensity of the background radiation source term. The high-temperature environment of the molten salt electrolyte presents further challenges for direct measurements. In situ instrumentation in pyroprocessing facilities is exposed to harsher radiation and temperature environments, which may result in instrumentation damage and drift during long-term deployment.

Aqueous-based systems typically employ pneumatic sampling of solutions at various stages, allowing for isolated analysis of solutions outside of the high-temperature and radiation environment. This approach is not directly applicable to pyroprocessing because the salt within the electrorefiner must be kept at elevated temperatures to prevent freezing. Thus, measurements need to either be conducted within high-temperature, high-radiation environments or obtained via representative sampling. While salt sampling via cold finger distillation<sup>7</sup> or microfluidic sampling<sup>8</sup> is possible, significant challenges still exist with respect to sampling methods. In the electrochemical processing flow sheet plutonium is distributed within the system as various chemical forms, including as an oxide powder, molten salt, and solid metal. The distribution of material between these forms can contribute to issues of sample inhomogeneity,<sup>9,10</sup> complicating sampling-based measurements. Likewise, the potential inhomogeneity of the electrolyte salt as a function of salt depth challenges representative sampling by any current sampling method.<sup>9</sup> Additionally, cold finger techniques are susceptible to melt crystallization,<sup>11</sup> resulting in fractional separation of fission products from the sample salt freezing process due to differences in melting points.<sup>7,11</sup>

Establishing a mass balance for electrochemical facilities is a significant challenge compared to aqueous facilities. An input mass balance immediately following dissolution within the input accountability tank (IAT) is central to existing aqueous-based PUREX flow sheets.<sup>12</sup> Because the input fuel is almost totally dissolved in aqueous solution within the IAT and is easily homogenized, representative sampling measurements can be taken at this stage in order to establish an input inventory. By contrast, the electrochemical separations flow sheet does not include an analogous dissolution or homogenization process at the head end and as a result cannot directly establish input accountancy measurements. While inferential techniques may be applied to estimate the mass balance (e.g., NDA measurements of UNF burnup signatures, allowing for estimation of plutonium receipts via depletion simulations), such techniques offer insufficient precision to close a mass balance on their own.<sup>12</sup>

As a result of these challenges, directly applying currently proposed and developed aqueous system safeguards to electrochemical flow sheets is presently viewed as impractical, necessitating alternative approaches to MC&A. Process monitoring and anomaly detection approaches have been proposed and studied as complements to traditional MC&A in both aqueous and electrochemical reprocessing facilities.<sup>13–15</sup> Process monitoring relies on in situ and near-real-time nondestructive measurements both to holistically monitor the operations of the facility and to track target elements and isotopes through the process. Near-term evaluation of this approach for MC&A and safeguards of electrochemical reprocessing facilities will rely on modeling and simulation of the overall facility and lab-scale demonstrations of limited scope.

Several models have been developed to model a production-scale electrochemical reprocessing facility. These simulation capabilities range from relatively simple flow sheet models that track material flows between static process blocks (such as the Separation and Safeguards Performance Model–Electrochemical, or SSPM-EChem model,<sup>2</sup> and other discrete-event simulation approaches<sup>16</sup>) to relatively sophisticated models capable of estimating dynamic material inventories at the cathode surface (Enhanced REFIN with Anodic Dissolution, or ERAD model<sup>17</sup>) and within the electrorefiner as a whole (Argonne Model for Pyrochemical Recycling–Dynamic Electrorefiner model, or AMPYRE-DyER model<sup>18</sup>). These simulation models of electrochemical reprocessing facilities provide a platform for simulating the response of potential monitoring and safeguards

measurements under a variety of conditions, including different source terms (e.g., UNF characteristics) and postulated diversion scenarios. Depending on the type of information tracked in the electrochemical system model, different safeguards measurements can be simulated. Here, the fundamental approach is to couple electrochemical process simulation to measurement response models governed either by physical first principles (e.g., radiological signatures) or semi-empirical correlations. Depending upon the information tracked in the simulation, this can include anything from elemental masses to isotopic distributions or even chemical characteristics, such as the distribution of oxidation states. Time-dependent material inventories are thus used to generate dynamic instrument responses to develop monitoring and safeguards approaches and evaluate their efficacy under protracted and abrupt diversion scenarios.

A variety of measurements have been proposed for application in pyroprocessing facilities. Section III section investigates many of these proposed measurements and evaluates key characteristics that may drive deployability and efficacy in an operating facility. Consideration is given to the ability to deploy measurements in electrochemical facility simulations based either on fundamental physical principles or correlation models derived from available experimental data.

### III. CANDIDATE MEASUREMENTS

Pyroprocessing involves several stages from dismantling UNF to product and waste form production. Throughout the system, material accountancy and process monitoring should be implemented to accurately track the amount and concentration of potential proliferation risks. A variety of measurements have been investigated and developed for potential deployment in pyroprocessing systems to meet this need. These proposed measurement methods are evaluated according to the information each technique may reveal about the process or material, the latency period, potential locations for measurement deployment, and the estimated uncertainty associated with the measurement. The surveyed measurement techniques are classified into three categories: passive radiation signatures, active radiation signatures, and control and process state variables. Each of these categories is discussed in the following subsections.

Candidate measurement technologies are evaluated according to (1) the information or feature of the physical system that can be assessed from the measurement in isolation, (2) the latency of making a measurement, (3) the locations in a typical pyroprocessing facility that the

measurement might be usefully deployed, and (4) the estimated measurement uncertainty reported in the open literature for the measurement technique. In this assessment, measurement latency is qualitatively judged and includes the entire process to make a single measurement, including potential sample preparation, measurement system setup, and measurement execution. Measurements that are taken in situ effectively instantaneously (i.e., seconds or less) are very low latency; measurements that are taken in situ but require significant counting time (i.e., minutes) are low latency; measurements that can be completed in hours are considered medium latency; measurements that require sampling and onsite testing (usually hours to days) are high latency; and finally, measurements that require sampling and offsite analysis (typically weeks to months) are very high latency. This evaluation is based on the authors' best understanding of likely deployment scenarios from the available literature and do not necessarily consider potential future developments to streamline longer latency measurements that are not currently well reported.

#### III.A. Passive Radiation Signatures

Passive radiation signatures, summarized in Table I, include passive gamma, neutron, and alpha measurements and calorimetry. Measuring passive radiation signatures is assumed to have a low latency time for detectors deployed in situ at target locations in the facility. If the harsh environment in situ precludes long-term deployment of detectors, then the latency of measurement will be governed by sampling technology to move representative material from the system to a suitable measurement environment.

##### III.A.1. Passive Gamma Measurements

Passive gamma detection plays an important role in UNF accountancy, particularly with respect to verifying input inventories of intact UNF assemblies via NDA (Ref. 4). Specifically, gamma spectroscopy can identify specific nuclides within UNF with strong characteristic signatures (such as  $^{137}\text{Cs}$ ,  $^{134}\text{Cs}$ , and  $^{154}\text{Eu}$ ) that can be directly correlated to the fuel discharge burnup and cooling time.<sup>37,38</sup> Moreover, contingent upon assumed knowledge of the burnup-to-enrichment correlation of the fuel (e.g., assuming of optimal economic use), such techniques can also be used to independently verify the totality of the enrichment, burnup, and cooling time.<sup>39,40</sup> From there, this information can then be employed using standard depletion codes to estimate the input plutonium content.<sup>24</sup>

In addition, continuous gamma spectroscopy measurements have been proposed as a process monitoring

TABLE I

Candidate Measurement Modalities for Electrochemical Process Monitoring and Safeguards: Passive Radiation Signatures

Measurement	Information Learned	Latency <sup>a</sup>	Locations	Estimated Uncertainty	References
Passive gamma Gross neutron	Fission product concentration (isotopic)	Low	Electrorefiner, U processing, U/TRU processing	1% to 2%	19 through 21
	Burnup	Low	Input accountancy	10%	20 through 24
	Input fuel burnup ( <sup>244</sup> Cm)	Low	Input accountancy	1% to 2%	20, 22, and 25
Alpha spectrometry	U/TRU isotope concentrations	Low	Electrorefiner, U processing, U/TRU processing	1%	19, 26 through 29
Calorimetry	Pu/Am assay	Medium	Input accountancy, electrorefiner, U processing, U/TRU processing	0.2% to 5%	30, 31, and 32
Microcalorimetry	Pu/Am isotope ratios	Medium	Input accountancy, U/TRU processing	<1%	33 through 36

<sup>a</sup>Latency conventions: Low = minutes and medium = hours.

technique for dissolved actinides in aqueous solution.<sup>41,42</sup> In similar fashion, given the accumulation of fission products within the eutectic salt, gamma spectroscopy can be used as a process indicator for features such as concentrations of alkaline earth and lanthanide-series fission products (both of which tend to be retained within the salt).

The estimated uncertainty of such techniques is usually within 10%, whether via spectroscopy or total counting methods.<sup>19,21</sup> Passive gamma measurements would likely be most effectively deployed at the electrorefiner, at the processing units for input accountancy, and as a confirmatory measurement at waste streams.

Gamma line energy emissions are among the most straightforward signatures to simulate given isotopic mass information within a flow sheet simulation. For a given isotopic mass  $N_k$ , line emissions can be calculated directly from fundamental data such as the Origen gamma/X-ray library per Eq. (1):

$$I_{\gamma}(E_i) = Y_i N_k \lambda_k \quad (1)$$

where

$\lambda_k$  = time constants

$E_i$  = emission energies

$Y_i$  = branching fractions for each unstable isotope tracked within Origen.<sup>43</sup>

An important limitation of this approach is that this does not itself provide information on detector response or other effects arising from radiation transport, which are typically considered computationally prohibitive to calculate in faster than real time during protracted diversion scenarios. Given this, the primary value in this approach to passive gamma signatures calculation is as a bounding estimate for the utility of gamma spectrographic information for tracking system behaviors; i.e., this information would most directly correlate with inventories of reactive fission products (primarily lanthanides) accumulating within the electrolyte salt. As such, it may serve as an indicator for diversion scenarios such as salt substitution (wherein actinide-bearing salt is diverted and replaced with clean salt).

In addition, the inclusion of a response function to approximate the detector response (e.g., a normal distribution with an estimated energy resolution parameter) could likewise be applied to this signature to approximate the response from measurements such as microcalorimetry arising from gamma and X-ray emissions from the sample. However, many of the same limitations given previously likewise apply here, i.e., a point estimate of emissions will not account for sample geometry effects (such as self-attenuation and the Compton background).

### III.A.2. Passive Neutron Measurements

Total neutron counting involves the quantification of three categories of neutrons: prompt and delayed neutrons

produced from spontaneous fission events and those from  $(\alpha, n)$  reactions that occur primarily in low- $Z$  material. Neutron counting can be more effective than gamma counting for estimating UNF burnup due to the greater attenuation of gamma rays compared to neutrons.<sup>20</sup> As a result, total neutron counting is generally more sensitive to small quantities of actinide materials, especially in matrices where gamma attenuation may be significant.<sup>25</sup>

Total neutron counting has long been used as a complementary means of burnup measurement for UNF assemblies (primarily arising from the spontaneous fission emissions by  $^{244}\text{Cm}$ ) (Ref. 22), particularly in combination with gross gamma counting or gamma spectroscopy.<sup>44</sup> Curium has been proposed as a tracer element to roughly monitor plutonium content in pyroprocessing based on the assumption that the elemental ratio of curium to plutonium remains fixed (i.e., that the two elements codeposit at the cathode at approximately the same rate).<sup>45</sup> However, quantifying this ratio within acceptable precision and accuracy to support safeguards decision making has proven a challenging task.<sup>10,46</sup> In particular, the spatial dependency of  $^{244}\text{Cm}$  atom density (given the nonuniform burnup profile of typical fuel assemblies) leads to a strong spatial dependence of the Pu-to- $^{244}\text{Cm}$  ratio through the fuel. This results in a relatively high sensitivity to granule and particle powder size in the chopping and voloxidation stages, resulting in a high statistical uncertainty.<sup>10</sup> More significantly, differences between the Gibbs free energy of formation of the actinides results in the extraction of Pu and Cm at different rates in the electrorefiner, challenging the assumption of a constant codeposition ratio.<sup>45,47,48</sup> As such, the use of  $^{244}\text{Cm}$  as a proxy for plutonium tracking has been generally determined to be unreliable as a safeguards measurement.<sup>45</sup>

Alternatively, the chemical makeup of the eutectic salt may offer the potential for direct plutonium quantification through  $(\alpha, n)$  emissions. Because of the relatively low atomic number of the salt constituents, preliminary studies have indicated that the intensity of  $(\alpha, n)$  neutron emissions from the electrorefiner may prove as strong as those arising from the spontaneous fission of  $^{244}\text{Cm}$  in some energy regimes.<sup>49</sup>

Total neutron counting could potentially indicate when neutron-emitting materials (primarily actinides) have been diverted. TRU materials from pyroprocessing would typically have a high neutron yield based on the curium and plutonium content; neutron counting could track the TRU product to ensure that direct diversion has not occurred. Similarly, total neutron counting can be employed as a confirmatory measurement to verify the nondiversion of

TRU materials into waste streams (i.e., by providing an upper bound on TRU content within such streams). However, substitution using neutron-emitting material is also a concern, to which neutron counting alone would not be sensitive.

The precision of total neutron counting typically spans between 1% and 2% error.<sup>25</sup> Areas of deployment for passive neutron counting include the electrorefiner, processing units, and for input accountancy as well as for confirmatory measurements at the waste streams.

For continuous-energy neutron emissions [such as spontaneous fission and medium-dependent  $(\alpha, n)$  reactions], a slightly more complex simulation approach must be undertaken based on tracked isotopic masses. The energy distribution of spontaneous fission neutrons is generally characterized via a Watt spectrum [Eq. (2)], wherein the distribution shape coefficients  $A$  and  $B$  are available in the Origen alpha decay library<sup>43</sup>:

$$\chi_k^{SF}(E) = R_k e^{-\frac{E}{A}} \sinh \sqrt{BE} \quad (2)$$

For neutrons arising from  $(\alpha, n)$  reactions, this source term is calculated via kinematic relationships and energy/medium-dependent stopping powers. Here, required nuclear data provided with Origen include the energy-dependent  $(\alpha, n)$  microscopic reaction cross sections (\*.ALPHAXS.DATA), energy states (i.e., ground, first excited, etc.) and branching ratios for recoil nuclei as a function of incident alpha energy (\*.ALPHAXS.DATA), and empirical stopping power cross-section fit coefficients (\*.STCOEFF.DATA) (Ref. 43).

The kinematic calculation for the emitted  $(\alpha, n)$  spectrum then follows the procedure outlined in the SOURCES 4C manual,<sup>50</sup> employing a thick-target medium approximation. For the electrorefiner vessel, it is generally assumed that the salt volume within the vessel far exceeds the average alpha particle range, making this a valid assumption.

Thus, the emitted  $(\alpha, n)$  spectrum can be calculated directly from the tracked inventory of alpha-emitting isotopes while making approximate assumptions of the fuel-to-salt ratio. Preliminary findings indicate that given the abundance of light elements in the eutectic salt (namely, lithium and chlorine),  $(\alpha, n)$  emissions may be a prominent component of the emitted neutron spectrum, chiefly from the decay of  $^{238}\text{Pu}$  and  $^{244}\text{Cm}$  (Ref. 49). Meanwhile, given that the SOURCES 4C procedure is implemented directly into Origen for medium-dependent  $(\alpha, n)$  (Ref. 43), these emission spectrum calculations can be easily validated via comparable Origen decay calculations.



### III.A.3. Alpha Spectrometry

In addition to neutrons and gamma rays, alpha particles are emitted from UNF by plutonium and other minor actinides. Analysis of alpha spectrometry can indicate the concentration of alpha-emitting isotopes in the measured volume. Much like gamma emissions, alpha decays from heavy nuclei occur at specific, known energies unique to each isotope with well-characterized yield fractions. As a result, alpha spectrometry can be used for isotopic analyses such as determining the ratio of  $^{240}\text{Pu}$  to  $^{239}\text{Pu}$ , which is useful for operational considerations (e.g., the ratio of fissile versus fertile plutonium content).<sup>28</sup>

The harsh environment within a pyroprocessing facility presents a challenging environment for passive detection; however, recently developed silicon carbide (SiC) alpha detectors can withstand such conditions.<sup>26,27</sup> This alpha detector can be deployed in the electrorefiner to monitor actinide concentrations in the salt or in the processing units to track material composition (with respect to alpha emitters). Sample-based alpha spectrometry typically has low uncertainty values that are usually in the range of 1% (Ref. 19). Moreover, work by Lukosi indicates that microfluidic channels within semiconductor-based alpha detectors (like SiC) can be used to limit the energy straggling effects arising from energy losses to the salt medium, thus affording greater ability to isolate specific line energy emissions.<sup>29</sup>

Research conducted by Garcia and continued by Taylor et al. resulted in the development of a 4H-SiC Schottky diode detector to track alpha particles within molten salt. This will provide information regarding actinide concentrations and give a good indicator of how well detectors operate when in contact with the salt.<sup>27</sup> The principle behind this detector's operation lies in its robust chemical stability in molten salt allowing for electrodeposition onto the sensor's surface much like would be seen onto one of the cathodes.<sup>51</sup> This eliminates the need for complex sample preparation and allows nondestructive evaluations to be made. Shielding within the electrorefiner is still of concern due to the thick radiation matrix, and thus a source containing the uranium and transuranic metal must be fabricated through extraction from the salt. Further study and development remains but preliminary results show that the 4H-SiC detector is accurately able to identify isotopes. It must be noted that this is the case in only some situations and not all due to the precision of the energy resolution for the detector.

To simulate alpha decay rates in the electrolyte, elemental mass ratios and isotopic distributions tracked at each location of interest can be combined with decay data

information from the SCALE alpha decay library (including line energy emission data and relative yields). Given known isotopic distributions, the emission intensity of alphas at energy  $E_i$  can be easily calculated per Eq. (3):

$$I_{\alpha}(E_i) = f_{\alpha} Y_i N_k \lambda_k \quad (3)$$

given fundamental data, such as the relative alpha yield to energy state  $i$  ( $Y_i$ ) and the fractional decay rate via alpha emission rather than spontaneous fission  $f_{\alpha}$ .

While the simulation of the alpha source term (and potentially even energy straggling behavior within the salt) is a relatively straightforward exercise, simulating the actual detector response includes a number of other factors, such as the charge collection efficiency. An example of this latter simulation benchmarking can be observed from Garcia. For this, they used the Sentaurus TCAD (a semiconductor simulation package using technology computer-aided design, or TCAD, simulations) to compare their detector to experimental data.<sup>27</sup> They found that the TCAD simulations did not match up with experimental results when it came to the temperature dependence of the charge collection. Parameters will need to be adjusted to improve the relationship between the model and temperature dependence. Given the state of this work, direct modeling of the alpha detector response within electrochemical flow sheet models may still be premature, but this nonetheless indicates promise for future modeling applications.

### III.A.4. Calorimetry

Calorimetry offers a near-real-time nondestructive method for assessing the fuel in bulk quantities. This technique uses heat emitted by decay radiation to quantify isotopic compositions usually from plutonium, curium, and americium via thermocouple devices.<sup>30,31</sup> Typical measurements involve the isolation of samples within a sealed thermocouple chamber connected to a large heat sink (i.e., a large block of thermally conductive material such as aluminum). The temperature difference induced by the sample relative to the environment produces a change in electrical potential (the Seebeck effect), and hence a measurable current; this change is proportional to the temperature gradient.<sup>31</sup> One drawback of calorimetry measurements is the relatively long latency, owing to the time required for the system to reach thermal equilibrium with the sample (which can be on the order of hours).<sup>30</sup>

A potential shortcoming of this method is that discrimination of different isotopes relies on a controlled, well-characterized measurement at normal operating conditions.

This doesn't present a major problem as the composition of the original nuclear fuel can be estimated in relation to its burnup and any deviation within it that would affect the measurement can be used to flag potential diversion scenarios.<sup>52</sup> If a well-characterized measurement is available, calorimetry is a likely candidate for input accountancy measurements. Even if the composition is unknown, calorimetry can be coupled with other techniques such as X-ray fluorescence (XRF) and neutron coincidence counting (NCC) to supplement the calorimetric measurement. Calorimetry could also be applied within the electrorefiner and the processing units of the facility.

Typical calorimetry uncertainty ranges from 5% to 7% due to the flow rate through the calorimeter and the temperature difference across the thermocouple.<sup>32</sup> However, small-sample calorimetry devices (operating in the megawatt range) with longer dwell times can achieve precision levels for relatively pure samples of Am and Pu of up to 0.2% (Ref. 30). Given the relatively high contributions of various medium-lived fission products to decay heat (e.g., <sup>137</sup>Cs, <sup>90</sup>Sr, etc.) along with their continuous accumulation within the salt, it is likely that such levels of precision would only be achievable for samples of the refined product stream (e.g., U/TRU recovered metal).

### III.A.5. Microcalorimetry

In contrast to traditional calorimetry measurements, which quantify material inventories via measurement of induced voltages from the Seebeck effect, microcalorimetry methods rely upon transition-edge sensors (TESs) operating within the superconduction regime.<sup>36</sup> These cryogenically cooled detectors can quantify single-photon heating by measuring the small increases in resistance within the TESs. This in turn produces electrothermal feedbacks that are measured by a superconducting quantum interface device (known as SQUID) ammeter capable of measuring the minute perturbations in the magnetic field.<sup>34,36</sup> In effect, microcalorimetry is designed to measure temperature changes due to interactions at the individual photon level and as such exhibits exceptional energy resolution (on the order of electron volts).<sup>33,34,36</sup> As a result, microcalorimetry is able to resolve X-ray features such as doublets from the  $K_{\alpha_2}$  transition that are indiscernible using traditional high-purity germanium (HPGe) gamma spectroscopy.

While traditional gamma-ray spectroscopy using HPGe detectors exhibits an energy resolution of around 400 to 500 eV, reported energy resolution for TES-based microcalorimetry systems has been reported to be as low as 1 to 2 eV full-width at half-maximum.<sup>33,36</sup> The very

fine energy resolution of TES-based microcalorimetry systems thus affords the ability to isolate elemental X-rays [the same as those used for measurements of elemental ratios in techniques such as XRF and high-resolution X-ray spectroscopy (HiRX)] from low-energy intrinsic gamma emissions characteristic of <sup>238</sup>Pu (99.853 keV), <sup>239</sup>Pu (98.78 keV), <sup>240</sup>Pu (104.23 keV), and <sup>241</sup>Am (98.97 and 102.98 keV) (Ref. 34). Notably, each of these gamma emissions are within a few kilo-electron-volts of K X-ray energies for U and Pu; thus it is only the added resolution afforded by these types of systems that allows for isotopic identification.

In principle, microcalorimetry measurements could be deployed at any stage of the pyroprocessing flow sheet, including for direct measurements of input isotopic ratios of Pu and Am from used fuel to be processed. However, because of the requirements for cryogenic cooling of the TES detector, measurements from the electrorefiner would require sampling (as the low-energy gammas of interest would likely be attenuated by the electrorefiner vessel wall). Alternatively, microcalorimetry would be expected to perform well in applications such as verification assay measurements of the U/TRU ingot (both as a process monitoring technique as well as an accountancy measurement), given its ability to characterize elemental and isotopic ratios of plutonium and americium.

Present limitations to the use of TES-based microcalorimetry systems come down to both their relatively small size and low count rate efficiency, along with the ability to construct sufficiently large systems for practical applications. Because TES detectors typically employ thicknesses on the sub-millimeter range (compared to on the order of centimeters for HPGe), their photopeak absorption efficiency is comparably smaller (about one-third of that from HPGe around 100 keV and rapidly dropping off at higher energies).<sup>34</sup> As a result of their small pixel size and lower efficiency, count rates are on the order of tens of counts per second (compared to thousands or even tens of thousands of counts per second for HPGe), thus requiring measurement times on the order of hours to achieve reliable statistics.<sup>35,36</sup>

The construction of megapixel-sized microcalorimeter systems would largely serve to overcome issues of low count rates, however a limiting factor here is in the efficient readout and multiplexing of signals from large pixel arrays.<sup>36</sup> Here, a fundamental limitation is in the bandwidth afforded by different multiplexing approaches, including from time-division, code-division, frequency-division, and microwave resonator-based approaches. (For greater technical details into the nature of these

approaches, the reader is directed to an excellent overview of each technique provided in Ref. 36.) Of these techniques, microwave resonator multiplexing offers the greatest potential in terms of bandwidth (and therefore array size), with the potential to reach hundreds of megahertz to several gigahertz (compared to the other approaches that are generally limited to around 10 MHz or less). A recent example of the microwave resonator-based approach achieved simultaneous readout of 128 individual TES pixels with a bandwidth of 1 GHz (Ref. 53). Further advancements in terms of signal processing capabilities can thus be expected to make facility-scale microcalorimetry systems more practical.

### III.B. Active Radiation Signatures

Active radiation signatures, summarized in Table II, include XRF, HiRX, k-edge densitometry (KED), hybrid

k-edge densitometry (HKED), active neutron interrogation (ANI), neutron coincidence multiplicity, inductively coupled plasma mass spectroscopy (ICP-MS), laser-induced breakdown spectroscopy (LIBS), Raman spectroscopy, near-infrared spectroscopy (Near-IR), and ultraviolet-visible spectroscopy (UV-Vis). The latency for these measurements varies significantly depending on the required sample preparation and counting time.

One important limitation to note with respect to simulating instrument responses for sampling-based techniques (e.g., X-ray-based techniques and LIBS) is that the reliability of such simulations are inherently limited to the fidelity of the flow sheet model itself. In other words, lacking detailed information on features such as the concentration profile as a function of depth, these models provide in effect a response based upon the average concentration within the salt over a given time interval. While insufficient for instrument design studies for

TABLE II

Candidate Measurement Modalities for Electrochemical Process Monitoring and Safeguards: Active Radiation Signatures

Measurement	Information Learned	Latency <sup>a</sup>	Locations <sup>b</sup>	Estimated Uncertainty	References
XRF	U/Pu ratios	Medium	Electrorefiner, U/TRU processing	1%	19, 31, 54, and 55
HiRX	U density	Medium	Electrorefiner, U processing, U/TRU processing	1%	56 and 57
KED		Medium		1%	54, 58, 59, and 60
HKED	U/Pu concentration (elemental)	Medium	Electrorefiner, U processing, U/TRU processing	<1%	54, 58, 59, and 60
LIBS	Elemental concentration	Low	Electrorefiner, U processing, U/TRU processing	5% to 10%	61 through 65
Active neutron interrogation	Fissile isotopes ( <sup>235</sup> U, <sup>239</sup> Pu, <sup>241</sup> Pu)	High	Electrorefiner, U processing, U/TRU processing	5%	19, 20, 66 through 70
Neutron coincidence multiplicity	<sup>240</sup> Pu mass	High	Electrorefiner, U processing, U/TRU processing	10%	71, 72, and 73
ICP-MS	Isotopic concentration	Very high	Electrorefiner	<1%	74 through 77
UV-Vis	An/Ln concentration	Medium	Electrorefiner, U processing, U/TRU processing	1% to 3%	78 through 81
Near-IR	Molecular concentration	Medium	Electrorefiner, U processing, U/TRU processing	1%	78, 79, and 82
Raman spectroscopy	Redox states	Medium	Electrorefiner, U processing, U/TRU processing	15%	83, 84, and 85

<sup>a</sup>Latency conventions: Low = minutes, medium = hours, high = days, very high = weeks or longer.

a specific facility design, this may still prove sufficiently useful for the characterization of the marginal efficacy of each of these techniques in timely detection of departures from normal operation conditions.

### III.B.1. X-Ray Interrogation

Two commonly proposed X-ray analysis techniques are XRF (and its corollary, HiRX) and KED. Analysis of XRF can quantify the ratio of plutonium and uranium concentrations, while that of KED indicates the absolute density of uranium in solution. Together, XRF and KED comprise HKED to quantify the absolute concentration of uranium and plutonium in solution. XRF and KED measurements would ideally take place at the electrorefiner, wherein actinides are dissolved into the fuel-salt mixture. Here, measurements of the X-ray transmission through the salt can be used to infer the absolute density of the majority actinide species (namely uranium) based on the characteristic drop in X-ray transmission around the k-edge absorption energy (which is directly proportional to the element concentration).

#### III.B.1.a. X-ray Fluorescence

X-ray fluorescence is a low-latency method based on active interrogation by an X-ray beam that can be used to determine the relative concentration of many isotopes within a UNF sample. This technique measures de-excitation X-rays emitted from ionized atoms to evaluate the relative elemental composition of the material.<sup>55</sup> XRF relies on the fact that the electron binding energies for each shell are unique to each element. When X-rays of high enough energy to overcome the electron binding energy ionize weakly bound K-shell electrons, an electron from a higher orbital (for example, the L-shell) can drop to fill the vacancy left by the liberated electron and a characteristic X-ray is emitted whose energy is equal to the difference in the binding energies of the two electron shells.<sup>55</sup> Because the electron binding energies are unique to each element, XRF spectra can be used to estimate elemental ratios based on the relative abundance of emitted fluorescence X-rays within an uncertainty of 1%. Measurement latency for XRF depends on whether the analysis is handled onsite or offsite. For onsite measurements and analysis, latency could be on the order of several hours, whereas for offsite analysis the required time could be several days.

#### III.B.1.b. High-Resolution X-ray

X-ray detection can also be done by using HiRX instrumentation, which is a spin-off from XRF. This

technique is based on monochromatic wavelength dispersive XRF, where doubly curved crystal optics are used for detection and excitation purposes to reduce interferences between closely spaced peaks.<sup>56</sup> The difference between this method and XRF is the high flux source being used to excite the sample in HiRX. The combination of a point-focusing excitation optic and a collection optic focuses and transmits specific X-ray energies to a sample, thereby allowing an investigator to strobe relatively narrow energy ranges.<sup>56</sup> Using such a technique provides a fast approach (several hours, if onsite) as little sample preparation is needed, with an uncertainty of 1% error.<sup>57</sup> This decrease in the amount of error is specifically important for diversion detection as the technique would be deployed within the electrorefiner and processing units for actinide detection, especially that of plutonium.

#### III.B.1.c. k-Edge Densitometry

A complementary technique to XRF is KED, which is a transmission-based measurement that measures the relative attenuation of an X-ray beam at the k-edge energy (where a characteristic rise in the photon absorption cross section is observed, as shown in Fig. 2) (Refs. 55 and 86). Thus the transmission of the X-ray beam through the sample is measured, which makes KED insensitive to radiation emitted by the sample. The resulting spectrum will show a drop at the k-edge energy when compared to the reference (incident) spectrum. The magnitude of this drop can be used to determine the uranium density in the measured sample and to tease out absolute

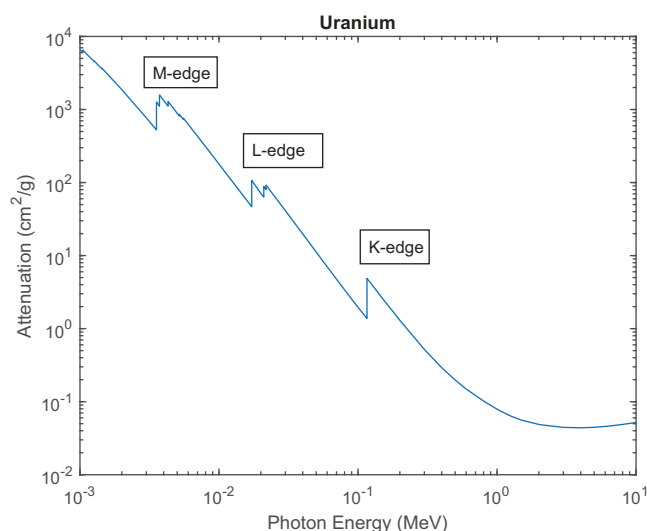


Fig. 2. Photon mass attenuation coefficients for uranium with atomic shell absorption edges indicated, based on data from Ref. 86.

abundances of minority species when combined with XRF in the form of HKED. The processing units are of particular interest as the HKED measurement would be a good indicator of the TRU concentrations as it maintains an uncertainty around 1%.<sup>19</sup> Measurement latency is similar to the values listed in [Sec. III.B.1.a](#), as the measurements can be combined and done at the same time.

#### III.B.1.d. Hybrid k-Edge Densitometry

Hybrid k-edge densitometry combines XRF and KED to estimate the absolute concentration of actinides, such as uranium and plutonium, within a solution. This is done by measuring the relative elemental concentrations via XRF, as well as inferring the dominant actinide density in the solution from the k-edge drop in the transmission spectrum.<sup>58</sup> Areas where this would be deployed include the electrorefiner and processing units. Typically a sample must be shipped to an offsite laboratory for analysis, but some facilities, such as the Rokkasho facility in Japan, already have HKED instrumentation implemented for aqueous reprocessing.<sup>12,60</sup> A moderate amount of latency may still remain for onsite instruments due to the requirements of sample collection and preparation but may be considered worth the investment considering the uncertainty is less than 1% ([Ref. 59](#)).

#### III.B.1.e. Modeling and Simulation of X-ray-Based Techniques: XRF, HiRX, and HKED

Hybrid k-edge densitometry is already presently deployed in aqueous reprocessing facilities such as Rokkasho-mura as part of their onsite analytical laboratory for measuring uranium and plutonium concentrations within the solvent.<sup>12</sup> Due to its potential ability to measure samples through optically thick materials, among other traits, HKED has been considered as a candidate technique for pyroprocessing measurements. A computational model of the HKED instrument at Oak Ridge National Laboratory based on elemental concentrations was developed by Cook and Skutnik using MCNP6.1 to simulate the interrogating X-ray spectra and subsequent k-edge attenuation and fluorescence X-ray generation.<sup>54</sup> This approach employed sequential MCNP simulations to first apply significant variance reduction (including forced collisions and deterministic transport regions) to achieve reasonable sampling of the X-ray spectrum reaching the terminus of each collimator region. From there, a second-stage simulation used the estimated X-ray spectra from the first stage to perform

analog transport to a detector volume in order to simulate the detector response.

The fuel composition inside the sample used by the MCNP model can be generated using depletion tools such as Origen. The model outputs the pulse height spectra for the KED and XRF aspects of HKED. From these, an empirical model of the detector response for both the k-edge drop and the relative ratios of fluorescence peaks can be developed to implement into electrochemical flow sheet models such as SSPM. The required elemental composition of the salt is already tracked in the SSPM and is available for use in a HKED subsystem. However, one open question specific to pyroprocessing is in the linearity (or lack thereof) of the  $\frac{Pu}{U}$  XRF ratio with respect to varying Pu and U concentrations. For example, the presence of additional actinide species may present overlaps in the XRF peaks used for elemental ratio determination, thereby introducing apparent nonlinearity in the response due to the overlap of individual XRF peaks.

Initial correlation studies using the MCNP model developed by Cook and Skutnik indicate a linear response to uranium concentration for the k-edge drop, confirming expectations.<sup>87</sup> Similarly, the XRF response for the intensity ratio between Pu and U  $K_{\alpha}$  lines follow a linear trend following a series of physical corrections accounting for factors that influence relative yields. These factors include the relative yields of emitted X-rays between the  $K_{\alpha_I}$  and  $K_{\alpha_{III}}$  lines as well as the ratio of the photoelectric absorption reaction rate.<sup>88</sup> Because fluorescence is a threshold-based reaction, the X-ray yield will be proportional to the integral of incident X-rays convoluted with the photoelectric absorption cross section ([Eq. 4](#)):

$$I^k(N_i) = Y_i^k \int_{E_{K_i}}^{\infty} \phi(E) \sigma_a^i(E) N_i dE \quad (4)$$

where

$Y_i^k$  = relative yield to X-ray state  $k$  for element  $i$  (i.e.,  $K_{\alpha_I}$  versus  $K_{\alpha_{III}}$ )

$E_{K_i}$  = k-edge energy for element  $i$  (i.e., the K-shell ionization energy)

$\phi(E)$  = interrogating X-ray flux spectrum  $\sigma_a^i$

$\sigma_a^i(E)$  = photoelectric absorption cross section for element  $i$

$N_i$  = atom density of elemental species  $i$  in solution.

As is evident from [Eq. \(4\)](#), because the ionization energy of the plutonium K-shell is slightly higher than

that of the uranium K-shell, this results in a slightly higher fluorescence per unit concentration (due to the slightly larger contributing energy range of the interrogating X-ray beam).

The estimated uncertainty in this calculation can be derived from the fitted slope of the line mapping the observed XRF peak ratio intensity [corrected per Eq. (4)] to the actual (simulated) concentration ratio. This estimate can then be used to inform a synthetic variation in the measurement approximating the true observed variation. The simulated response  $I(x_i)$  can thus be perturbed assuming a normal distribution about the calibration curve [Eq. (5)]:

$$I(x_i) = m_i x_i + b_i + N(0, \sigma_i) \quad (5)$$

where

- $x_i$  = concentration of element  $i$  (known to the flow sheet model)
- $m_i$  = slope coefficient of the calibration curve element  $i$
- $b_i$  = intercept coefficient of the calibration curve element  $i$ .

### III.B.2. Laser-Induced Breakdown Spectroscopy

Laser-induced breakdown spectroscopy is a real-time, nondestructive measurement technique that performs elemental analysis by employing a high-powered, pulsed laser to vaporize small material samples (including solids, liquids, and aerosols), producing a transient plasma.<sup>61</sup> Upon relaxation, the ions emit photons at characteristic elemental frequencies, thus allowing for identification of the elemental composition of the sample.<sup>62</sup> In this sense, LIBS is somewhat analogous to XRF-based techniques, given their common dependence on secondary photons arising from electron de-excitations.

Laser-induced breakdown spectroscopy was first proposed for electrochemical sampling measurements because it can be performed at significant distance from its intended target, potentially simplifying its implementation and potentially allowing for deployment above the electrorefiner vessel.<sup>62–65</sup> LIBS has been considered for both in situ<sup>63</sup> and ex situ<sup>65</sup> deployment. The deployment scenario would drive latency of measurement (low for in situ measurements and medium to high for ex situ).

Initial results of a potential ex situ deployment showed a high relative standard deviation (around 5% to 10%), likely due to dust buildup on the sensor or

possible other effects such as laser energy fluctuations or fractional crystallization.<sup>7,65</sup> For in situ deployment, there are still some concerns about laser impact on the surface of the molten salt. The laser will cause temporary localized distortion of the liquid salt (splashes, ripples, etc.), which implies a minimum recovery time between laser pulses and a tuning of laser duration and intensity.

Much like X-ray-based techniques (XRF, HiRX, and HKED), the instrument response from LIBS is expected to be linearly proportional to individual elemental concentrations within the salt solution. Such a finding is supported by experimental studies in glove-box studies using both uranium and actinide surrogate materials. Williams et al. developed and tested linear calibration curves for uranium spectral lines for an aerosol-LIBS measurement (at 367.01, 385.96, and 387.10 nm), reporting that they achieved accurate calibration curves via linear regression analysis<sup>64</sup>; similar results were likewise reported for Ce and Gd (55.2- and 564.2-nm lines, respectively) used as U/Pu surrogates.<sup>65</sup> As such, these response curves (along with their estimated limit of detection) could in principle be used to simulate the instrument response within a flow sheet model. Similar to X-ray-based measurements, a synthetic uncertainty estimate can be produced by perturbing the calibration curve response with a normal distribution [Eq. (5)], using the estimated fit uncertainty as the standard deviation. Given that multiple emission lines are used for identifying elemental species, each response curve would thus be independently modeled.

Notably, the calibration curves such as those reported by Williams et al. represent a correlated response to a specific instrument and measurement apparatus. Thus, while features such as the wavelengths used for fitting would translate to other systems, features of the response curve may vary. Moreover, uncertainty estimates derived by empirical correlations to these data include calibration-specific systematic sources of uncertainty (e.g., variations in the laser power, aerosol droplet size distribution, etc.). As such, the utility of these curves is primarily in producing an informed estimate of the relative sensitivity of this method to changes in system conditions (and hence, its ability to contribute to the detection of both abrupt and protracted diversion scenarios).

### III.B.3. Active Neutron Interrogation

Active neutron interrogation involves bombarding a sample with neutrons to induce fission.<sup>20</sup> Appropriate neutron-sensitive detectors are combined with timing

information (such as from coincidence gating) in order to discriminate induced fission neutrons from the neutron source [typically ( $\alpha,n$ ) sources like AmBe, AmLi, or PuBe].

Active neutron interrogation differs from passive techniques as the response doesn't depend only on the fission neutrons from the sample, but also on the neutrons that originate from the interrogating source.<sup>70</sup> Investigation into ANI for assay of uranium is ongoing due to the small spontaneous fission contribution to passive neutron emissions of uranium compared to other isotopes. ANI typically offers an uncertainty of about 5%, but a very high latency period in regard to being able to identify isotopic concentrations.<sup>19</sup> Potential sampling locations include the electrorefiner and cathode processing units.

### III.B.4. Neutron Coincidence Counting

Neutron coincidence counting can be used passively or actively and measures the almost instantaneous prompt neutrons to obtain unique signatures of isotopes and the spontaneous fission rate within a given material.<sup>73,89</sup> NCC uses the measurement of singles and (coincident) doubles count rates to quantify plutonium content (typically  $^{240}\text{Pu}_{\text{eff}}$ ) within a sample.<sup>73</sup>

The disadvantage of NCC is the high latency period since often samples taken from the electrorefiner and processing units must be sent to a lab for analysis. This method usually has an accuracy of 10% and may not be a reliable method to account for material in a timely manner.<sup>72</sup>

### III.B.5. Inductively Coupled Plasma Mass Spectrometry

Inductively coupled plasma mass spectrometry also supports quantification of isotopic concentrations. This technique ionizes a sample with a laser of inductively coupled plasma. From there the plasma is extracted through a series of cones and mass spectrometry is applied to separate ions according to their mass-to-charge ratio and to simultaneously/near simultaneously identify the amount of each isotope in the sample. The distinction is based on whether a time-of-flight (TOF) or multicollector (MC) method ICP-MS device is used. The isotopic ratios are analyzed using a known standard for comparison.

There are multiple subcategories of ICP-MS, but the most predominant of these are the TOF and MC methods. In TOF, ions at different mass-to-charge ratios ( $m/z$ ) are not measured simultaneously.<sup>77</sup> Instead they are measured in a rapid sequence with little compromise

between the number of  $m/z$  values monitored.<sup>77</sup> The sample material is ionized and sent around a track, with the time required to reach the detector logged. This can lead to less precision but detection is still able to occur if longer-duration laser ablation pulses, or many smaller pulses, are used. Conversely, the MC device can monitor up to eight  $m/z$  values simultaneously at one setting of the magnetic field and accelerating voltage. The MC device does this by bending ion trajectories similar to a calutron, and determining the  $m/z$  value based off of the impact site on the detector. The MC device is used for higher-precision measurements.<sup>77</sup>

Inductively coupled plasma mass spectrometry isotopic quantification would be useful within the electrorefiner due to the high concentration of various isotopes within the salt, especially uranium and plutonium. A downside to this technique is the extensive sample preparation time that is required,<sup>75</sup> making ICP-MS less attractive as a real-time measurement method. ICP-MS requires taking a sample, and then transporting that sample to a facility capable of performing ICP-MS. This facility can be onsite, however, it still will require some sample preparation analysis time.<sup>77</sup> With that said, if done properly ICP-MS measurements have among the highest precision of available techniques, capable of quantifying individual isotopes with typical uncertainties of no greater than 2% and usually lower than 1% (Ref. 74).

### III.B.6. Optical Measurements

Various classes of optical absorption spectroscopy can be applied to determine the lanthanide and actinide composition of nuclear fuel within the electrorefiner and processing units. Both groups form stable complex ionic species and have highly responsive energy levels to the spacing of surrounding material groups.<sup>79</sup> Thus, these optical measurements track the TRU products throughout the system by using gaps between molecular orbitals to quantify concentration. Three real-time medium latency sampling techniques have been proposed. The first two, UV-Vis and Near-IR use specific wavelengths of light to gather information about the molecules in a mixture. The third method, Raman spectroscopy, uses light of multiple wavelengths to identify elements.

#### III.B.6.a. UV-Vis Spectroscopy

As its name implies, UV-Vis uses light from the UV region of the spectrum, approximately wavelengths of

330 to 900 nm, to identify certain elements.<sup>78</sup> The principle behind this method is that certain materials deflect or absorb certain wavelengths of light. This absorption or deflection is based on the gap between molecular orbitals. The lower the energy gap the more likely electrons can be excited and thus the beam of light becomes more attenuated.<sup>79</sup> With the use of a spectrophotometer, one can calculate the concentration of a material such as uranium in eutectic salt via optical transmission measurements,<sup>90</sup> yielding elemental concentrations of actinides and lanthanides. Researchers at the Korea Atomic Energy Research Institute successfully showed that they could detect rare earth elements in a LiCl-KCl molten salt.<sup>91</sup> This holds an advantage over other analysis techniques such as ICP-MS as it can be done in situ. Experiments have been conducted by Park et al. examining the online monitoring of uranium and rare earth concentrations using UV-Vis. The results showed the calibration curves for the selected absorption peak positions provided good linearity and reasonable detectable concentrations.<sup>90</sup> The uncertainty in this type of measurement is generally between 1% and 3% (Ref. 80).

### III.B.6.b. Near-IR Spectroscopy

Similar to UV-Vis, Near-IR measures the light absorption for the lanthanides and actinides in a mixture to determine the quantity of said material. Unlike UV-Vis, Near-IR uses infrared light, approximately wavelengths of 900 to 1700 nm (Ref. 78). The equipment of a spectrophotometer is the same but yields a slightly better uncertainty in the overall measurement, typically below 1% due to the different wavelengths of the measured light.<sup>78</sup> In general, most instruments designed for UV-Vis spectroscopy are simultaneously capable of Near-IR measurements.

### III.B.6.c. Raman Spectroscopy

Raman spectroscopy uses light of various wavelengths (including UV, infrared, and visible) to project a laser onto a substance and then measure the energy shift of the scattered light.<sup>85</sup> Raman spectroscopy is similar to UV-Vis and Near-IR in that the measurement involves a comparison of before and after incidence, although energy shifts are measured instead of intensity. The energy shift results from vibrational shifts from the molecules of the material. Each element will give a different corresponding shift and thus leads to elemental identification over the lanthanide and actinide groups. Thus, it is

also similar to LIBS except Raman spectroscopy uses a low-energy pulse where LIBS requires a high enough energy to exceed the ablation threshold. Therefore, it is possible to use a single instrument setup to combine Raman and LIBS if a short time delay is between the successive pulses.<sup>92</sup> Raman spectroscopy is of particular interest within the salt of the electrorefiner, which holds multiple elements, to account for its complex composition. One advantage Raman spectroscopy has over UV-Vis and Near-IR is its ability to measure from a stand-off distance; that is, direct contact is not necessary. A result of this is the uncertainty is often much higher, typically 10% to 15% (Ref. 84).

### III.B.6.d. Modeling and Simulation of Optical Measurements

Optical techniques are designed to probe features at the molecular level (i.e., chemical bonds), thus giving an indication as to the distribution of redox states within the electrolyte. Because of the multiple stable redox states available to actinides such as U and Pu, characterization of the relative distribution of states may serve as another useful process indicator.

Experiments by Harrington and Sundheim at New York University have sought to measure complex ions in a bath of LiCl-KCl molten salt.<sup>79</sup> The first transition series was particularly looked at to determine how susceptible it is to vibrational patterns through a medium. These complex ions could be identified in most cases by comparing the measured spectra to those with features known to belong to the target ions.<sup>79</sup> This gives a foundation for the spectra results that should be obtained when using optical measurements.

Simulation of the measurement response of optical methods relies on the availability of oxidation state information for relevant elements. These data could be theoretically inferred in existing electrochemical reprocessing simulation models in terms of the oxidized and reduced states of U ( $U^{4+}$  and  $U^{3+}$ ) via calculation of the surface concentration during the reversible and irreversible cathodic and anodic regions as a function of the electrode potential and the integral applied current<sup>93</sup> and using known quantities such as the formal electrode potential  $E^0$  and other known or measured quantities (such as the diffusion coefficients of the oxidant and reductant species). Here it is assumed the bulk  $UCl_3$  comprises the initial concentration at the irreversible cathodic region; from this, the  $U^{4+}$  concentration can be directly calculated for the irreversible anodic region.<sup>93</sup>



Given a calculation of the time-dependent oxidant and reductant species within the electrolyte [calculated as part of the cyclic voltammetry (CV) model], it becomes possible to infer the distribution of ionic states and thus the characteristic responses of optical transmission measurements.

### III.C. Control and Process State Variable Monitoring

Control and process state variables include nonradiation-based bulk measurements of the physical process. Control variables refer to the measurement and monitoring of parameters of the physical process that incites separations; in the case of electrochemical processing these are primarily electrical in nature. Process state variables include nonradiation characteristics of the process operation (e.g., level, mass, temperature). The control and process state variable signals, summarized in Table III, include CV, electrical signatures, load cell mass measurements, electromanometer measurements, salt level and density, temperature, and off-gas monitors.

#### III.C.1. Cyclic Voltammetry

Electrical signatures of interest that can be readily measured can be combined to perform voltammetric techniques, such as CV (others include pulse and square wave voltammetry), by monitoring the current resulting from an applied potential.<sup>97</sup> Within the electrorefiner, a potential is induced that then controls the concentrations of the redox species at the electrode surface and the rate of the reaction, all in accordance with the Nernst and Butler-Volmer laws.<sup>96,97</sup> Mass migration of ions occurs due to the induced electric field created between the electrodes. From there the concentrations of certain materials, mainly actinides, can be inferred within the solution by plotting the current versus potential and observing peaks associated with known redox potentials. The Nernst equation explains the relationship between potential force being applied and the redox concentrations at the surface of the electrode. The Butler-Volmer equation relates electrical current on an electrode to the induced electrode potential.<sup>97</sup> To obtain the current signature, a transformer can be used to take a changing current signal from a primary winding and provide a magnetic field coupled

TABLE III

Candidate Measurement Modalities for Electrochemical Process Monitoring and Safeguards: Operations and Control

Measurement	Information Learned	Latency <sup>a</sup>	Locations	Estimated Uncertainty	References
Cyclic voltammetry	U, Pu, TRU concentration (elemental)	Low	Electrolytic reduction, electrorefiner, salt processing, U/TRU drawdown	10%	93 through 100
Electromanometer	Level, volume, density	Very low	Electrorefiner, U processing, U/TRU processing	0.05% to 1%	13
Salt level	Bulk accountancy	Very low	Electrolytic reduction, electrorefiner, salt processing, U/TRU drawdown	1%	101 through 104
Double/triple bubbler	Salt level, density	Very low	Electrolytic reduction, electrorefiner, salt processing, U/TRU drawdown	0.16% to 3%	101, 103, and 104
Load cell	Mass	Very low	Input accountancy, output accountancy, electrorefiner, U processing, U/TRU processing, U/TRU drawdown	0.05%	13 and 105
Off-gas monitors	Fission product gases (e.g., I, Xe, Kr)	Low	Oxide reduction, electrorefiner	5%	13 and 106

<sup>a</sup>Latency conventions: Very low = seconds, low = minutes.

into secondary windings.<sup>107</sup> Then the induced secondary current can be measured by other machines such as an ammeter. This replicated current is proportional to the one being measured and allows isolation from the main voltage line. Next, a voltmeter is used by measuring the potential difference between two points within a circuit. This is a rapid real-time measurement on the order of seconds and gives an uncertainty in inferred actinide concentration of about 10% (Refs. 97, 108, and 109).

The Idaho National Laboratory is currently undergoing experiments using a molten salt solvent to test the experimental procedure when using voltammetry as a viable measurement technique. The goal is to help determine which type of voltammetry is most applicable and a general understanding between the current and elemental reduction peaks.<sup>94</sup> If this experiment is successful, a library can be compiled exhibiting the ratio between elemental concentration and current that could be used in simulation models. Here, accountancy signatures would be obtained by relating the peak current values to the corresponding bulk concentrations of actinides.

Pouri et al. have likewise proposed methods for predicting current and voltage trace curves by starting from a diffusion model of the electrolyte behavior (relying upon the calculated diffusion properties of targeted materials from published literature)<sup>100</sup> as well as direct predictions from operating conditions using machine learning methods.<sup>93</sup>

For the diffusion modeling approach, the concentration of extracted species as a function of time (along with the current and voltage) is calculated directly by solving the integral equations (as a function of integrated current applied over time) governing the surface concentrations of extracted species at the cathode and electrode.<sup>93</sup> Pouri and Phongikaroon then derive the solution for the potential for the reversible and irreversible conditions of the cathodic and anodic regions; with this known, it is then straightforward to calculate the current for the reversible and irreversible components.<sup>93</sup> Here what is assumed is the thermophysical properties of the extracted species (i.e., diffusion coefficients for the oxidant and reductant species and the formal electrode potentials) inferred from experimental measurements. A limitation of this approach however is that the root mean squared error (rmse) increases as the concentration of the extracted species increases.<sup>93</sup>

For the latter case, Pouri et al. developed a multi-layer perceptron artificial neural network (ANN) model based on a very large set of CV trace training data (consisting of over 231 000 individual data points).<sup>100</sup>

The proposed model generates a current-voltage trace as a function of input electrode potential, process time, element concentrations, and scan rate.<sup>100</sup> Here, their investigation focused upon finding a neural net structure capable of minimizing the amount of data required to produce a viable training set (i.e., to avoid “overfitting” by the neural network model) while simultaneously minimizing residual error, namely by controlling the number of hidden layers and neurons at each layer.<sup>100</sup> Their most robust model [employing a (9, 10, 15)-18 structure] resulted in an RMSE of around 0.3% to 4.4% over a range of 0.5% to 5% (weight percent) concentration of  $ZrCl_3$  in the eutectic salt, indicating that the ANN approach may be a viable mechanism for synthetic prediction of CV traces from operational data.<sup>100</sup> For comparison, the rmse for current and voltage for the diffusion-based model ranged from about 0.76% and 1.8% for current and voltage, respectively, at 1% weight fraction up to 9.1% and 6.3% at 5% weight fraction.<sup>93</sup> Thus, for purposes of representative and timely modeling of CV for online monitoring purposes, an ANN approach based on operating conditions at and elemental concentrations in the electrorefiner may prove preferable to a first-principles approach at the expense of potentially failing to capture cases far outside the training data.

### III.C.2. Bulk Measurements

Process monitoring can include any bulk measurement within a facility measured in situ, that is, nonsampling measurement techniques.<sup>13</sup> Nonradiation-based process monitoring measurements include level and density measurements, load cell mass measurements, off-gas monitors, current, voltage, and temperature. All of these quantities are relatively straight forward to capture and provide a real-time (low-latency) indication of the operational state of the system as a whole.

#### III.C.2.a. Level and Density Measurements

Level and density on their own do not indicate the composition of material in the reprocessing system; however, level can indicate the gross diversion or addition of material in key locations while density can give an indication of changes in composition that may result from postulated substitution scenarios. These measurements can be performed via direct measurement of the salt within the electrorefiner, processing units, and draw-down, and as salt moves through the salt purification process. This can be done through tank measurements

where a measurement will determine the position of salt level relative to the top or bottom of the tank.<sup>102</sup> Level and density measurements are commonly proposed through the use of a double or triple bubbler<sup>101,103,104</sup> or with an electromanometer.<sup>13</sup>

In the case of measurements of the electrolyte salt, the variability of the salt surface tension must also be taken into account in order to ensure accurate density measurements. For example, prior studies have indicated a bias of around 3% for density measurements for double bubbler systems, largely attributable to varying salt surface tension, characteristic of differences in salt temperature, and dissolved fission product content.<sup>103</sup> By adding a third tube, it is thus possible to additionally quantify the effect of surface tension, thereby improving the accuracy of the pneumatic measurements of level and density for molten salt systems.<sup>104</sup> Validation experiments for the performance of the triple bubbler system in both aqueous- and salt-based solutions found that the addition of surface tension measurements improved the estimated accuracies for density and level to 0.16% and 0.31%, respectively, with a 3.38% maximum deviation for the estimated surface tension.<sup>104</sup>

### III.C.2.b. Load Cell

Load cell measurements use an electrical signal to proportionally measure the magnitude of an applied force such as a compressive force.<sup>105</sup> Similar to the level and density measurements, no quantification of material composition or concentration is obtained from load cell measurements alone. Rather, load cell measurements indicate the overall mass moving through the system, which may be useful to detect some postulated diversion scenarios. This type of measurement can be applied at almost every area within the pyroprocessing facility, including the electrorefiner, the processing units, the drawdown, and input and output accountancy. The uncertainty associated with load cell is roughly 0.05% but can increase due to hardware issues, such as incorrect mounting or equipment damage.<sup>13</sup>

### III.C.2.c. Off-Gas Monitors

Off-gas monitors measure noble gases and volatile fission product gases in real time to quantify the bulk mass balance of material through the pyroprocessing cycle<sup>106</sup>; however, this measurement does not indicate elemental or isotopic concentrations. By measuring the released gas, both fission products and particular reaction rates can be proportionally quantified.<sup>13</sup>

Off-gas monitors can be implemented at the electrolytic reducer to quantify the oxygen release for a bulk mass balance<sup>13</sup> and the voloxidation stage to measure activities of noble gases and volatile fission products, which can be correlated back to fuel receipts. Off-gas monitors can also be used to determine if abnormal or unexpected gases are being released to better protect against some postulated substitution scenarios.

Significant research has been reported to develop sensors and instrumentation for monitoring electrochemical reprocessing facilities. A comprehensive process monitoring and safeguards approach would combine many of these technologies deployed throughout a facility; development and evaluation of such a framework requires a robust data set representative of the range of expected operating conditions (e.g., UNF characteristics). A production-scale electrochemical reprocessing facility does not currently exist to support operational data collection, and an experimental campaign to provide all of the data necessary on the same set of samples would require a significant investment of both money and time. In the absence of representative operational and synchronous experimental data, modeling and simulation of the reprocessing facility and the associated measurement techniques can provide the data necessary for proof-of-principle demonstration and initial monitoring and safeguards framework development.

## IV. SUMMARY

The electrochemical reprocessing flow sheet presents a number of challenges to conventional approaches to material accountancy developed for aqueous-based flow sheets. In particular, because of the incomplete extraction of materials within the electrorefiner stage, pyroprocessing flow sheets maintain a continuous inventory of special nuclear materials. As a result, maintaining timeliness goals for material accountancy using traditional mass-balance methods may be infeasible without system cleanouts and detailed inventory taking performed at an impractical frequency (i.e., on the order of monthly). As a result, alternative MC&A approaches may prove more practical and effective, such as low-latency process monitoring approaches that focus on departures from expected operating conditions conducted alongside (higher-latency) confirmatory measurements.

In this paper we have sought to explore the range of available measurement techniques that may be applicable to pyroprocessing facility measurements. These measurements fall roughly into one of three categories: (1) passive radiation signatures, (2) active (elicited) radiation signatures

(via gamma or neutron interrogation), and (3) control and process state variables. In general, while passive radiation measurements like passive gamma spectroscopy provide relatively low latency in measurements, the level of precision associated with these measurements is likely insufficient on its own to achieve facility MC&A goals. By contrast, active interrogation techniques may be capable of providing relatively high precision for material quantification at the cost of higher latency. Hence, this class of measurements may prove useful for confirmatory measurements designed to reduce uncertainties in in situ material inventories but cannot by themselves be expected to provide timely detection of material diversion and other anomalies. However, these techniques form a basis for methods to possibly be introduced into safeguards performance models for electrochemical separations facilities. By incorporating a diverse set of measurement techniques, it becomes possible to synthesize orthogonal physical signatures (such as neutron, gamma, and thermodynamic properties), thereby providing a defense in depth and ensuring that no single technique's weakness is a liability. In short, by correlating different types of measurements at various locations within the flow sheet, it therefore may be possible to achieve acceptably low uncertainty in estimates of material inventories to facilitate longer separation campaigns.

Beyond quantifying available measurement technologies and their respective latency and precision, we have also sought to characterize measurements by the type of information revealed (e.g., isotopic, elemental, or other types of composition information) as well as their most favorable locations for deployment within an electrochemical separations flow sheet. For example, active interrogation techniques would most likely be predicated on sample collection, implying that these measurements would primarily target stages such as the electrorefiner vessel and product streams. Passive radiation measurements may prove to be more versatile (depending upon the desired information to be obtained), warranting placement throughout the facility, including at the input accountancy stage, within the electrorefiner, and at the product streams. Finally, operational characteristics (such as measurements of the salt density, level/mass, and off-gas characteristics) may serve as complementary measures used for correlating state information inferred from radiological measurements throughout the facility.

Along these lines, we have likewise summarized the means by which a subset of these measurements may be simulated within facility safeguards models, including the physical information required to conduct these assessments. For example, beginning with time-dependent elemental separation factors at various stages one can layer isotopic

information over material flows by calculation of the UNF source term (i.e., via depletion calculations). With the isotopic and elemental source terms known, it becomes possible to calculate passive radiological emissions from fundamental nuclear data, including contributions from gammas, betas, alphas, and neutrons. With respect to the latter category, contributions from both the spontaneous fission source term as well as  $(\alpha, n)$  neutrons may yield distinct physical information about plutonium content within the electrorefiner vessel.

Other types of measurement responses, including HKED and CV, may be possible to simulate via semi-empirical correlations from prior experimental and computational studies (again based upon in-process inventories). Beyond these categories, additional types of measurements (such as optical transmission measurements like UV-Vis and Near-IR spectroscopy) would require additional chemical state information about the system (i.e., information about the distribution of oxidation states of actinides within the electrolyte). While it is conceivable that such information may be included in higher-fidelity process models (or potentially derived from electrotransport calculations of chemical species at the anode and cathode regions), this is presently beyond the scope of most available electrochemical separations facility models presently available.

## Acknowledgments

This work was supported by a Nuclear Energy University Programs grant sponsored by the U.S. Department of Energy, Office of Nuclear Energy, award number DE-NE0008553. The authors likewise wish to gratefully acknowledge the support and assistance of Benjamin Cipiti and Nathan Shoman of the Sandia National Laboratory.

## ORCID

Jamie B. Coble  <http://orcid.org/0000-0002-0736-673X>

## References

1. H. E. GARCIA et al., "Application of Process Monitoring to Anomaly Detection in Nuclear Material Processing Systems via System-centric Event Interpretation of Data from Multiple Sensors of Varying Reliability," *Ann. Nucl. Energy*, **103**, 60 (2017); <https://doi.org/10.1016/j.anucene.2017.01.006>.
2. B. B. CIPITI et al., "Modeling and Design of Integrated Safeguards and Security for an Electrochemical Reprocessing Facility," SAND2012-9303, Sandia National Laboratories (2012); <https://doi.org/10.2172/1055891>.

3. M. F. SIMPSON, “Developments of Spent Nuclear Fuel Pyroprocessing Technology at Idaho National Laboratory,” INL/EXT-12-25124, Idaho National Laboratory (2012); <https://doi.org/10.2172/1044209>.
4. H. LEE et al., “Current Status of Pyroprocessing Development at KAERI,” *Sci. Technol. Nucl. Ins.*, **2013**, 1 (2013); <https://doi.org/10.1155/2013/343492>.
5. J.-H. YOO et al., “A Conceptual Study of Pyroprocessing for Recovering Actinides from Spent Oxide Fuels,” *Nucl. Eng. Technol.*, **40**, 7, 581 (2008); <https://doi.org/10.5516/NET.2008.40.7.581>.
6. T. RILEY, C. POPE, and R. BENEDICT, “Safeguards Performance Model for Evaluation of Potential Safeguards Strategies Applied to Pyroprocessing Facilities,” *Nucl. Eng. Des.*, **301**, 157 (2016); <https://doi.org/10.1016/j.nucengdes.2016.02.035>.
7. J. R. VERSEY, S. PHONGIKAROON, and M. F. SIMPSON, “Separation of CsCl from LiCl-CsCl Molten Salt by Cold Finger Melt Crystallization,” *Nucl. Eng. Technol.*, **46**, 3, 395 (2014); <https://doi.org/10.5516/NET.06.2013.082>.
8. M. G. POLLACK, V. K. PAMULA, and R. B. FAIR, “Methods for Performing Microfluidic Sampling,” US Patent 7,759,132 (2010).
9. K. KINOSHITA et al., “Separation of Actinides from Rare Earth Elements by Means of Molten Salt Electrorefining with Anodic Dissolution of U-Pu-Zr Alloy Fuel,” *J. Phys. Chem. Solids*, **66**, 2–4, 619 (2005); <https://doi.org/10.1016/j.jpics.2004.06.069>.
10. S. M. WOO, S. S. CHIRAYATH, and M. FRATONI, “Nuclide Composition Non-Uniformity in Used Nuclear Fuel for Considerations in Pyroprocessing Safeguards,” *Nucl. Eng. Technol.*, **50**, 7, 1120 (2018); <https://doi.org/10.1016/j.net.2018.05.011>.
11. J. ULRICH and H. BÜLAU, “Melt Crystallization,” *Handbook of Industrial Crystallization*, Chap. 7, 2nd ed., pp. 161–179, A. S. MYERSON, Ed., Butterworth-Heinemann (2002); <https://doi.org/10.1016/B978-075067012-8/50009-4>.
12. R. BEAN, “Aqueous Processing Material Accountability Instrumentation,” INL/EXT-07-13431, Idaho National Laboratory (2007); <https://doi.org/10.2172/923487>.
13. B. CIPITI, “Process Monitoring Considerations for Reprocessing,” *Proc. Institute of Nuclear Materials Management 56th Annual Mtg.*, Desert Springs, California, July 12–16, 2015; <https://www.osti.gov/scitech/biblio/1256551SAND2015-4416C> (current as of Sep. 19, 2019).
14. D. RAPPLEYE, “Developing Safeguards for Pyroprocessing: Detection of a Plutonium Co-Deposition on Solid Cathode in an Electrorefiner by Applying the Signature-Based Safeguards Approach,” Master’s Thesis, North Carolina State University (2012); <http://www.lib.ncsu.edu/resolver/1840.16/8350> (current as of Sep. 19, 2019).
15. A. G. le COQ, “Design of a Safeguards Instrument for Plutonium Quantification in an Electrochemical Refining System,” Master’s Thesis, Texas A&M University (2013); <http://hdl.handle.net/1969.1/151148> (current as of Sep. 19, 2019).
16. R. BORRELLI, M. TOLMAN, and J. LEE, “Preliminary Analysis of Facility Design for Pyroprocessing Safeguardability,” *Trans. Am. Nucl. Soc.*, **116**, 197 (2017).
17. R. M. CUMBERLAND and M.-S. YIM, “Development of a 1D Transient Electrorefiner Model for Pyroprocess Simulation,” *Ann. Nucl. Energy*, **71**, 52 (2014); <https://doi.org/10.1016/j.anucene.2014.03.028>.
18. L. E. MAGGOS et al., “Update on Electrochemical Mass Balance Modeling for Safeguards,” ANL/FCRD-MPACT/2015-9-2, Argonne National Laboratory (2015); <https://www.osti.gov/servlets/purl/1350096> (current as of Sep. 19, 2019).
19. L. A. CURRIE, “Quantifying Uncertainty in Nuclear Analytical Measurements,” IAEA-TECDOC-1401, International Atomic Energy Agency, Vienna, Austria (2004); <http://www-pub.iaea.org/MTCD/publications/PDF/te1401web.pdf> (current as of Sep. 19, 2019).
20. J. DOYLE, *Nuclear Safeguards, Security and Nonproliferation*, Butterworth-Heinemann (2008).
21. P. DeFelice, “Uncertainty in Gamma Spectrometry,” National Institute of Metrology of Ionizing Radiation, Italy (2007); <http://indico.ictp.it/event/a06186/session/54/contribution/35/material/0/0.pdf> (current as of Sep. 19, 2019).
22. J. R. PHILLIPS, *Irradiated Fuel Measurements*, Chap. 18, pp. 529–562, NUREG/CR-5550, LA-UR-90-72, Washington, DC (1991).
23. M. TARVAINEN et al., “NDA Techniques for Spent Fuel Verification and Radiation Monitoring,” *STUK document STUK-YTO-TR*, **131** (1997).
24. I. C. GAULD and M. W. FRANCIS, “Investigation of Passive Gamma Spectroscopy to Verify Spent Nuclear Fuel Content,” presented at 51st Annu. INMM Mtg., Baltimore, Maryland, July 11–15, 2010.
25. J. SPRINKLE, “Total Neutron Counting Instruments and Applications,” *Passive Nondestructive Assay Manual-PANDA*, Chap. 15, pp. 435–456 (1991).
26. A. ZELASKI, “Development of a Silicon Carbide Schottky Diode Detector for Use in Determining Actinide Inventories Based on Alpha Particle Spectroscopy,” Master’s Thesis, The Ohio State University (2011); <http://rave.ohiolink.edu/etdc/view?accnum=osu1316486528>.

27. T. GARCIA, “Fabrication, Characterization and Simulation of 4H-SiC Schottky Diode Alpha Particle Detectors for Pyroprocessing Actinide Monitoring,” PhD Thesis, The Ohio State University (2014); <http://rave.ohiolink.edu/etdc/view?accnum=osu1387490688>.
28. S. K. AGGARWAL, “Alpha-Particle Spectrometry for the Determination of Alpha Emitting Isotopes in Nuclear, Environmental and Biological Samples: Past, Present and Future,” *Anal. Methods*, **8**, 27, 5353 (2016); <https://doi.org/10.1039/C6AY00920D>.
29. E. LUKOSI, “Microfluidic Alpha Spectrometry of UOX PWR UNF in a Molten Salt,” *Nucl. Sci. Eng.*, **188**, 3, 294 (2017); <https://doi.org/10.1080/00295639.2017.1367248>.
30. H. TAGZIRIA et al., “Absolute Determination of Small Samples of Pu and Am by Calorimetry,” *Nucl. Instrum. Methods Phys. Res., Sect. A*, **691**, 90 (2012); <https://doi.org/10.1016/j.nima.2012.06.062>.
31. S. ABOUSAHL et al., “Radiometric Assay Techniques for the Control of Minor Actinides in Advanced Nuclear Fuel Cycles,” *Proc. 24th ESARDA*, Luxembourg, 2002, p. 138 (2015).
32. “Uncertainty of Calorimeter Measurements at NREL’s High Flux Solar Furnace,” presented at ASME Int. Solar Energy Conf., Maui, Hawaii, April 4–8, 1992; <http://www.nrel.gov/docs/legosti/old/4593.pdf> (current as of Sep. 19, 2019).
33. J. N. ULLOM et al., “Optimized Transition-Edge X-ray Microcalorimeter with 2.4 eV Energy Resolution at 5.9 keV,” *Appl. Phys. Lett.*, **87**, 19, 194103 (2005); <https://doi.org/10.1063/1.2061865>.
34. A. S. HOOVER et al., “Determination of Plutonium Isotopic Content by Microcalorimeter Gamma-Ray Spectroscopy,” *IEEE Trans. Nucl. Sci.*, **60**, 2, 681 (2013); <https://doi.org/10.1109/TNS.2013.2249091>.
35. A. S. HOOVER et al., “Uncertainty of Plutonium Isotopic Measurements with Microcalorimeter and High-Purity Germanium Detectors,” *IEEE Trans. Nucl. Sci.*, **61**, 4, 2365 (2014); <https://doi.org/10.1109/TNS.2014.2332275>.
36. J. N. ULLOM and D. A. BENNETT, “Review of Superconducting Transition-Edge Sensors for X-ray and Gamma-Ray Spectroscopy,” *Supercond. Sci. Technol.*, **28**, 8, 084003 (2015); <https://doi.org/10.1088/0953-2048/28/8/084003>.
37. C. WILLMAN et al., “Nondestructive Assay of Spent Nuclear Fuel with Gamma-Ray Spectroscopy,” *Ann. Nucl. Energy*, **33**, 5, 427 (2006); <https://doi.org/10.1016/j.anucene.2005.12.005>.
38. S. CARUSO et al., “Validation of  $^{134}\text{Cs}$ ,  $^{137}\text{Cs}$  and  $^{154}\text{Eu}$  Single Ratios as Burnup Monitors for Ultra-High Burnup  $\text{UO}_2$  Fuel,” *Ann. Nucl. Energy*, **34**, 1–2, 28 (2007); <https://doi.org/10.1016/j.anucene.2006.11.009>.
39. A. FAVALLI et al., “Determining Initial Enrichment, Burnup, and Cooling Time of Pressurized-Water-Reactor Spent Fuel Assemblies by Analyzing Passive Gamma Spectra Measured at the Clab Interim-fuel Storage Facility in Sweden,” *Nucl. Instrum. Methods Phys. Res., Sect. A*, **820**, 102 (2016); <https://doi.org/10.1016/j.nima.2016.02.072>.
40. J. COBLE, C. ORTON, and J. SCHWANTES, “Multivariate Analysis of Gamma Spectra to Characterize Used Nuclear Fuel,” *Nucl. Instrum. Methods Phys. Res., Sect. A*, **850**, 18 (2017); <https://doi.org/10.1016/j.nima.2017.01.030>.
41. C. R. ORTON et al., “Proof of Concept Simulations of the Multi-Isotope Process Monitor: An Online, Nondestructive, Near-Real-Time Safeguards Monitor for Nuclear Fuel Reprocessing Facilities,” *Nucl. Instrum. Methods Phys. Res., Sect. A*, **629**, 1, 209 (2011); <https://doi.org/10.1016/j.nima.2010.10.024>.
42. C. R. ORTON et al., “Proof of Concept Experiments of the Multi-Isotope Process Monitor: An Online, Nondestructive, Near Real-time Monitor for Spent Nuclear Fuel Reprocessing Facilities,” *Nucl. Instrum. Methods Phys. Res., Sect. A*, **672**, 38 (2012); <https://doi.org/10.1016/j.nima.2011.12.083>.
43. “SCALE: A Modular Code System for Performing Standardized Computer Analyses for Licensing Evaluations,” ORNL/TM-2005/39, Version 6.2.3 ed., Radiation Safety Information Computational Center, Oak Ridge National Laboratory (2018).
44. S. VACCARO et al., “A New Approach to Fork Measurements Data Analysis by RADAR-CRISP and ORIGEN Integration,” *IEEE Trans. Nucl. Sci.*, **61**, 4, 2161 (2014); <https://doi.org/10.1109/TNS.2014.2320604>.
45. M. GONZALEZ et al., “Application of a One-Dimensional Transient Electrorefiner Model to Predict Partitioning of Plutonium from Curium in a Pyrochemical Spent Fuel Treatment Process,” *Nucl. Technol.*, **192**, 2, 165 (2015); <https://doi.org/10.13182/NT15-28>.
46. R. A. BORRELLI, “Use of Curium Spontaneous Fission Neutrons for Safeguardability of Remotely-Handled Nuclear Facilities: Fuel Fabrication in Pyroprocessing,” *Nucl. Eng. Des.*, **260**, 64 (2013); <https://doi.org/10.1016/j.nucengdes.2013.03.025>.
47. T. TODA et al., “Thermodynamic Properties of Lanthanides and Actinides for Reductive Extraction of Minor Actinides,” *J. Nucl. Sci. Technol.*, **46**, 1, 18 (2009); <https://doi.org/10.1080/18811248.2007.9711502>.
48. A. OSIPENKO et al., “Electro-Chemistry of Curium in Molten Chlorides,” *Recent Trends in Electrochemical Science and Technology*, InTech, Rijeka, 11 (2012).
49. N. GILLIAM, J. COBLE, and S. SKUTNIK, “ $(\alpha, n)$  Source Terms as a Novel Signature for Pyroprocessing Safeguards,”

- Proc. Advances in Nuclear Nonproliferation Technology and Policy Conf.*, Orlando, Florida, November 2018.
50. W. WILSON et al., “SOURCES 4C: A Code for Calculating (alpha,n), Spontaneous Fission, and Delayed Neutron SOURCES and Spectra,” LA-UR-02-1839, Los Alamos National Laboratory (2002); <https://permalink.lanl.gov/object/tr?what=info:lanl-repo/lareport/LA-UR-02-1839> (current as of Sep. 19, 2019).
  51. N. R. TAYLOR et al., “Isotopic Concentration of Uranium from Alpha Spectrum of Electrodeposited Source on 4H-SiC Detector at 500°C,” *J. Radioanal. Nucl. Chem.*, **320**, 2, 441 (2019); <https://doi.org/10.1007/s10967-019-06492-y>.
  52. Y. ANDO, K. NISHIHARA, and H. TAKANO, “Estimation of Spent Fuel Compositions from Light Water Reactors,” *J. Nucl. Sci. Technol.*, **37**, 10, 924 (2000); <https://doi.org/10.1080/18811248.2000.9714974>.
  53. J. A. B. MATES et al., “Simultaneous Readout of 128 X-ray and Gamma-Ray Transition-Edge Microcalorimeters Using Microwave SQUID Multiplexing,” *Appl. Phys. Lett.*, **111**, 6, 062601 (2017); <https://doi.org/10.1063/1.4986222>.
  54. M. T. COOK, “Hybrid K-edge Densitometry as a Method for Materials Accountancy Measurements in Pyrochemical Reprocessing,” PhD Dissertation, University of Tennessee (2015); [https://trace.tennessee.edu/utk\\_graddiss/3329](https://trace.tennessee.edu/utk_graddiss/3329).
  55. M. C. MILLER, “X-Ray Fluorescence,” *Passive Nondestructive Assay Manual-PANDA*, Chap. 10, pp. 313–336 (1991); <http://www.lanl.gov/orgs/n/n1/panda/00326405.pdf> (current as of Sep. 19, 2019).
  56. K. McINTOSH, G. HAVRILLA, and S. REILLY, “Determination of Plutonium in Spent Nuclear Fuel Using High Resolution X-ray,” *Spectrochim. Acta Part B At. Spectrosc.*, **110**, 91 (2015); <https://doi.org/10.1016/j.sab.2015.05.014>.
  57. G. HAVRILLA et al., “Initial HiRX Performance Characterization of Pu in Spent Nuclear Fuel Matrix,” presented at the Symp. Int. Safeguards: Linking Strategy, Implementation and People, Vienna, Austria, October 20–24, 2014; <https://www.iaea.org/safeguards/symposium/2014/home/e-proceedings/sg2014-papers/000142.pdf> (current as of Sep. 19, 2019).
  58. E. ESBELIN, “Actinide L-Line ED-XRF and Hybrid K-Edge Densitometer Spectra Processing,” presented at the IAEA Symp. Int. Safeguards: Linking Strategy, Implementation and People, Vienna, Austria, October 20–24, 2014; <https://www.iaea.org/safeguards/symposium/2014/home/e-proceedings/sg2014-papers/000062.pdf> (current as of Sep. 19, 2019).
  59. H. OTTMAR and H. EBERLE, “The Hybrid K-Edge/K-XRF Densitometer: Principles-Design-Performance,” KFK-4590, Institut für Kernphysik, Karlsruhe, Germany (1991); <https://publikationen.bibliothek.kit.edu/270030394> (current as of Sep. 19, 2019).
  60. A. BERLIZOV et al., “A Quantitative Monte Carlo Modelling of the Uranium and Plutonium X-ray Fluorescence (XRF) Response from a Hybrid K-Edge/K-XRF Densitometer,” *Nucl. Instrum. Methods Phys. Res., Sect. A*, **615**, 1, 127 (2010); <https://doi.org/10.1016/j.nima.2010.01.010>.
  61. J. FENG et al., “Study to Reduce Laser-Induced Breakdown Spectroscopy Measurement Uncertainty Using Plasma Characteristic Parameters,” *Spectrochim. Acta Part B*, **65**, 7, 549 (2010); <https://doi.org/10.1016/j.sab.2010.05.004>.
  62. N. SMITH, J. SAVINA, and M. WILLIAMSON, “Application of Laser Induced Breakdown Spectroscopy to Electrochemical Process Monitoring of Molten Chloride Salts,” presented at the Symp. Int. Safeguards: Linking Strategy, Implementation and People, Vienna, Austria, October 20–24, 2014; <https://www.iaea.org/safeguards/symposium/2014/home/e-proceedings/sg2014-papers/000200.pdf> (current as of Sep. 19, 2019).
  63. A. N. WILLIAMS and S. PHONGIKAROON, “Laser-Induced Breakdown Spectroscopy (LIBS) in a Novel Molten Salt Aerosol System,” *Appl. Spectrosc.*, **71**, 4, 744 (2017); <https://doi.org/10.1177/0003702816648965>.
  64. A. WILLIAMS and S. PHONGIKAROON, “Laser-Induced Breakdown Spectroscopy (LIBS) Measurement of Uranium in Molten Salt,” *Appl. Spectrosc.*, **72**, 7, 1029 (2018); <https://doi.org/10.1177/0003702818760311>.
  65. A. WILLIAMS, K. BRYCE, and S. PHONGIKAROON, “Measurement of Cerium and Gadolinium in Solid Lithium Chloride–Potassium Chloride Salt Using Laser-Induced Breakdown Spectroscopy (LIBS),” *Appl. Spectrosc.*, **71**, 10, 2302 (2017); <https://doi.org/10.1177/0003702817709298>.
  66. R. E. MARRS et al., “Fission-Product Gamma-Ray Line Pairs Sensitive to Fissile Material and Neutron Energy,” *Nucl. Instrum. Methods Phys. Res. A*, **592**, 3, 463 (2008); <https://doi.org/10.1016/j.nima.2008.04.032>.
  67. M. T. ANDREWS et al., “MCNP6 Simulations of Gamma Line Emissions from Fission Products and Their Comparisons to Plutonium and Uranium Measurements,” *Prog. Nucl. Energy*, **79**, 8795 (2015); <https://doi.org/10.1016/j.pnucene.2014.11.012>.
  68. J. KNOWLES et al., “A Generalized Method for Characterization of  $^{235}\text{U}$  and  $^{239}\text{Pu}$  Content Using Short-Lived Fission Product Gamma Spectroscopy,” *Nucl. Instrum. Methods Phys. Res., Sect. A*, **833**, 38 (2016); <https://doi.org/10.1016/j.nima.2016.06.112>.
  69. T. NICOL et al., “Feasibility Study of  $^{235}\text{U}$  and  $^{239}\text{Pu}$  Characterization in Radioactive Waste Drums Using Neutron-Induced Fission Delayed Gamma Rays,” *Nucl. Instrum. Methods Phys. Res., Sect. A*, **832**, 85 (2016); <https://doi.org/10.1016/j.nima.2016.06.055>.

70. M. CLAPHAM et al., “Performance Comparison of Different Active Neutron Interrogation Techniques for Safeguards Applications,” *Proc. 19th Annual Symp. Safeguards and Nuclear Material Managements (ESARDA 97)*, p. 359, Montpellier, France (1997).
71. “Safeguards Techniques and Equipment,” 2011 ed., no. 1 in *International Nuclear Verification Series*,” Rev. 2, International Atomic Energy Agency (2011).
72. N. DYTLEWSKI, M. KRICK, and N. ENSSLIN, “Measurement Variances in Thermal Neutron Coincidence Counting,” *Nucl. Instrum. Methods Phys. Res. A*, **327**, 2–3, 469 (1993); [https://doi.org/10.1016/0168-9002\(93\)90713-R](https://doi.org/10.1016/0168-9002(93)90713-R).
73. N. ENSSLIN, “Principles of Neutron Coincidence Counting,” *Passive Nondestructive Assay Manual-PANDA*, Chap. 16, pp. 457–492; <http://www.lanl.gov/orgs/n/n1/panda/00326411.pdf> (current as of Sep. 19, 2019).
74. V. BARWICK, S. ELLISON, and B. FAIRMAN, “Estimation of Uncertainties in ICP-MS Analysis: A Practical Methodology,” *Anal. Chim. Acta*, **394**, 2–3, 281 (1999); [https://doi.org/10.1016/S0003-2670\(99\)00302-5](https://doi.org/10.1016/S0003-2670(99)00302-5).
75. G. GEHRELS, V. VALENCIA, and J. RUIZ, “Enhanced Precision, Accuracy, Efficiency, and Spatial Resolution of U-Pb Ages by Laser Ablation-Multicollector-Inductively Coupled Plasma-Mass Spectrometry,” *Geochem. Geophys. Geosyst.*, **9**, 3 (2008); <https://doi.org/10.1029/2007GC001805>.
76. J. I. G. ALONSO et al., “Determination of Fission Products and Actinides in Spent Nuclear Fuels by Isotope Dilution Ion Chromatography Inductively Coupled Plasma Mass Spectrometry,” *J. Anal. At. Spectrom.*, **10**, 5, 381 (1995); <https://doi.org/10.1039/JA9951000381>.
77. R. S. HOUK et al., “Comparison of Time-of-Flight and Multicollector ICP Mass Spectrometers for Measuring Actinides in Small Samples Using Single Shot Laser Ablations,” IS-5162/US0605867, Ames Laboratory (2005); <https://doi.org/10.2172/892796>.
78. O. A’AMAR, R. LEY, and I. BIGIO, “Comparison Between Ultraviolet-Visible and Near-Infrared Elastic Scattering Spectroscopy of Chemically Induced Melanomas in an Animal Model,” *J. Biomed. Opt.*, **9**, 6, 1320 (2004); <https://doi.org/10.1117/1.1803845>.
79. G. HARRINGTON and B. SUNDHEIM, “Absorption Spectra in Molten Salts,” *Ann. N.Y. Acad. Sci.*, **79**, 11, 950 (1960); <https://doi.org/10.1111/j.1749-6632.1960.tb42767.x>.
80. L. SOOVALI et al., “Uncertainty Sources in UV-Vis Spectrophotometric Measurement,” *Accredit. Qual. Assur.*, **11**, 6, 246 (2006); <https://doi.org/10.1007/s00769-006-0124-x>.
81. C. SCHROLL et al., “Absorption Spectroscopy for the Quantitative Prediction of Lanthanide Concentrations in the 3LiCl-2CsCl Eutectic at 723 K,” *Anal. Methods*, **8**, 43, 7731 (2016); <https://doi.org/10.1039/C6AY01520D>.
82. P. SHAW et al., “Improved Near-Infrared Spectral Responsivity Scale,” *J. Res. Nat. Inst. Stand. Technol.*, **105**, 5, 689 (2000); <https://www.ncbi.nlm.nih.gov/pmc/articles/PMC4872696>.
83. A. S. HAKA et al., “Determination of Uncertainty in Parameters Extracted from Single Spectroscopic Measurements,” *J. Biomed. Opt.*, **12**, 6, 1 (2007); <https://doi.org/10.1117/1.2815692>.
84. T. BEECHEM, L. YATES, and S. GRAHAM, “Error and Uncertainty in Raman Thermal Conductivity Measurements,” *AIP Rev. Sci. Instrum.*, **86**, 4 (2015); <https://doi.org/10.1063/1.4918623>.
85. K. KNEIPP et al., “Ultrasensitive Chemical Analysis by Raman Spectroscopy,” *Chem. Rev.*, **99**, 10, 2957 (1999); <http://pubs.acs.org/doi/abs/10.1021/cr980133r>.
86. M. BERGER, “XCOM: Photon Cross Sections Database,” (2010); <http://www.nist.gov/pml/data/xcom/index.cfm> (current as of Sep. 19, 2019).
87. M. COOPER, S. SKUTNIK, and J. MITCHELL, “A Semi-Empirical HKED Model for Pyroprocessing Safeguards Evaluation,” *Proc. Advances in Nuclear Nonproliferation Technology and Policy Conf. (ANTPC 2018)*, Orlando, Florida, November 2018.
88. J. MITCHELL et al., “Source Term Development and Response Analysis for HKED Simulation in Electrochemical Reprocessing,” *Proc. Advances in Nuclear Nonproliferation Technology and Policy Conf. (ANTPC 2018)*, Orlando, Florida, November 2018.
89. S. CROFT et al., “Feasibility of Classic Multiplicity Analysis Applied to Spent Nuclear Fuel Assemblies,” LA-UR-11-03303, Los Alamos National Laboratory (2011).
90. Y. PARK et al., “UV-Vis Absorption Spectroscopic Study for On-Line Monitoring of Uranium Concentration in LiCl-KCl Eutectic Salt,” *Microchem. J.*, **99**, 2, 170 (2011); <https://doi.org/10.1016/j.microc.2011.04.013>.
91. J. LEE, “Development of In-Situ UV-Vis Technique for the Molten Salt Electrorefining Process of Uranium,” *Trans. Korean Nuclear Society Autumn Mtg.* (2005); <https://www.kns.org/files/prepaper/17/476.pdf> (current as of Sep. 19, 2019).
92. V. N. LEDNEV et al., “Combining Raman and Laser Induced Breakdown Spectroscopy by Double Pulse Lasing,” *Anal. Bioanal. Chem.*, **410**, 1, 277 (2018); <https://doi.org/10.1007/s00216-017-0719-6>.
93. S. R. POURI and S. PHONGIKAROON, “An Interactive Reverse-Engineering Cyclic Voltammetry for Uranium Electrochemical Studies in LiCl-KCl Eutectic Salt,” *Nucl. Technol.*, **197**, 3, 308 (2017); <https://doi.org/10.1080/00295450.2016.1273730>.



94. C. W. JOHNSON, M. L. DUNZIK-GOUGAR, and S. X. LI, “On-Line Monitoring of Actinide Concentrations in Molten Salt Electrolyte,” *Trans. Am. Nucl. Soc.*, **95**, 1, 129 (2006); <https://indigitallibrary.inl.gov/sites/sti/sti/3562838.pdf> (current as of Sep. 19, 2019).
95. H. HAYASHI, M. AKABORI, and K. MINATO, “Cyclic Voltammetry Behavior of Americium at a Liquid Cadmium Electrode in LiCl-KCl Eutectic Melts,” *Nucl. Technol.*, **162**, 2, 129 (2008); <http://epubs.ans.org/?a=3939>.
96. M. PEOVER and B. WHITE, “The Electro-Oxidation of Polycyclic Aromatic Hydrocarbons in Acetonitrile Studied by Cyclic Voltammetry,” *J. Electroanal. Chem.*, **13**, 1–2, 93 (1967); [https://doi.org/10.1016/0022-0728\(67\)80097-4](https://doi.org/10.1016/0022-0728(67)80097-4).
97. S. KOUNAVES, “Voltammetric Techniques,” *Handbook of Instrumental Techniques for Analytical Chemistry*, pp. 709–725, F. A. SETTLE, Ed., Prentice Hall (1997).
98. C. SCHROLL et al., “Spectroelectrochemistry of EuCl<sub>3</sub> in Four Molten Salt Eutectics; 3 LiCl-NaCl, 3 LiCl-2 KCl, LiCl-RbCl, and 3 LiCl-2 CsCl; at 873 K,” *Electroanalysis*, **28**, 9, 2158 (2016); <https://doi.org/10.1002/elan.201600048>.
99. C. SCHROLL et al., “Electrochemistry and Spectroelectrochemistry of Europium(III) Chloride in 3LiCl-2KCl from 643 to 1123 K,” *Anal. Chem.*, **85**, 20, 9924 (2013); <https://doi.org/10.1021/ac402518p>.
100. S. R. POURI, M. MANIC, and S. PHONGIKAROON, “A Novel Framework for Intelligent Signal Detection via Artificial Neural Networks for Cyclic Voltammetry in Pyroprocessing Technology,” *Ann. Nucl. Energy*, **111**, 242 (2018); <https://doi.org/10.1016/j.anucene.2017.09.002>.
101. J. SIEGWARTH, “Measurement Uncertainties of Level Gages for Liquefied Natural Gas,” NBSIR 82-1668, National Bureau of Standards (1982); <https://www.gpo.gov/fdsys/pkg/GOVPUB-C13-0bcc98fd473d97376cf2f6ff9aa369b3/pdf/GOVPUB-C13-0bcc98fd473d97376cf2f6ff9aa369b3.pdf> (current as of Sep. 19, 2019).
102. H. HOPPER, “Leak/Level: A Dozen Ways to Measure Fluid Level and How They Work,” *Sensors* (2004); <http://www.sensormag.com/sensors/leak-level/a-dozen-ways-measure-fluid-level-and-how-they-work-1067> (current as of Sep. 19, 2019).
103. H. LAMBERT, “Study of a Double Bubbler for Material Balance in Liquids,” INL/EXT-13-29609, Idaho National Laboratory (2013); <https://www.osti.gov/scitech/servlets/purl/1097166> (current as of Sep. 19, 2019).
104. A. N. WILLIAMS, G. G. GALBRETH, and J. SANDERS, “Accurate Determination of Density, Surface Tension, and Vessel Depth Using a Triple Bubbler System,” *J. Ind. Eng. Chem.*, **63**, 149 (2018); <https://doi.org/10.1016/j.jiec.2018.02.011>.
105. F. BOURGEOIS and G. BANINI, “A Portable Load Cell for In-Situ Ore Impact Breakage Testing,” *Int. J. Miner. Process.*, **65**, 1, 31 (2002); [https://doi.org/10.1016/S0301-7516\(01\)00057-6](https://doi.org/10.1016/S0301-7516(01)00057-6).
106. K. MURAKAMI, Y. YUASA, and T. ITO, “Off-Gas Monitor,” Japan Patent Document 62-6199/A/ (1987).
107. B. YARBOROUGH, “Components and Methods for Current Measurement,” (2012); <https://www.powerelectronics.com/power-electronics-systems/components-and-methods-current-measurement> (current as of Sep. 19, 2019).
108. D.-H. KIM et al., “Real-Time Monitoring of Metal Ion Concentration in LiCl-KCl Melt Using Electrochemical Techniques,” *Microchem. J.*, **114**, 261 (2014); <https://doi.org/10.1016/j.microc.2014.01.011>.
109. D. YOON and S. PHONGIKAROON, “Measurement and Analysis of Exchange Current Density for U/U<sup>3+</sup> Reaction in LiCl-KCl Eutectic Salt via Various Electrochemical Techniques,” *Electrochim. Acta*, **227**, 170 (2017); <https://doi.org/10.1016/j.electacta.2017.01.011>.